Stochastic model for detection of signals in noise

Stanley A. Klein* **and Dennis M. Levi**

School of Optometry, University of California, Berkeley, Berkeley, California 94720, USA
**Corresponding author: sklein@berkeley.edu*

Received June 19, 2009; revised October 2, 2009; accepted October 5, 2009;
posted October 5, 2009 (Doc. ID 113069); published October 30, 2009

Fifty years ago Birdsall, Tanner, and colleagues made rapid progress in developing signal detection theory into a powerful psychophysical tool. One of their major insights was the utility of adding external noise to the signals of interest. These methods have been enhanced in recent years by the addition of multipass and classification-image methods for opening up the black box. There remain a number of as yet unresolved issues. In particular, Birdsall developed a theorem that large amounts of external input noise can linearize nonlinear systems, and Tanner conjectured, with mathematical backup, that what had been previously thought of as a nonlinear system could actually be a linear system with uncertainty. Recent findings, both experimental and theoretical, have validated Birdsall's theorem and Tanner's conjecture. However, there have also been experimental and theoretical findings with the opposite outcome. In this paper we present new data and simulations in an attempt to sort out these issues. Our simulations and experiments plus data from others show that Birdsall's theorem is quite robust. We argue that uncertainty can serve as an explanation for violations of Birdsall's linearization by noise and also for reports of stochastic resonance. In addition, we modify present models to better handle detection of signals with both noise and pedestal backgrounds. © 2009 Optical Society of America

OCIS codes: 330.4060, 330.5510.

1. INTRODUCTION

It is fitting for this special issue commemorating Birdsall and Tanner to explore, in depth, the topic of the detection of signals in noise. "Google" Birdsall and Tanner and see the richness of the research on this topic in the mid-1950s to 1960s at the University of Michigan. Ted Cohn, a student there in the latter part of that era, edited a book, *Visual Detection* [1], with a multiplicity of articles by Tanner, Birdsall, and dozens of others. The articles are remarkable in their depth and sophistication, and it makes one wonder whether much new has been accomplished in the past 50 years. The present article will focus on an important contribution from Ted Birdsall that is known as Birdsall's theorem, and in the process we will examine the general topic of modeling the detection of signals in both noise and known backgrounds.

Birdsall's theorem has relevance to any study of detection of signals in noise. A concise statement of the theorem was given by Lasley and Cohn [2], p. 275: "According to Birdsall's Theorem, when the variance of any source of noise prior to the nonlinear transducer is large enough so that other sources of noise in an experiment can be neglected, the resulting d' psychometric function will be linear." A mathematical derivation of Birdsall's theorem was provided by Lasley and Cohn (Appendix A) [2]. It can be understood by considering a simple nonlinear system with external noise:

$$y(c_{\text{test}}, \sigma_{\text{ext}}) = (c_{\text{test}} + \sigma_{\text{ext}}\mathbf{R}_1)^{\gamma} + \sigma_{\text{int}}\mathbf{R}_2, \tag{1}$$

where c_{test} is the contrast of the test pattern, σ_{ext} and σ_{int} are the external and internal noise standard deviations, and $\mathbf{R}_i$ is a Gaussian random number with a mean of zero and unity standard deviation. Three cases can be distinguished:

Case 1. If σ_{ext} is negligible then by the definition of d' we have $d' = {c_{\text{test}}}^{\gamma}/\sigma_{\text{int}}$, the ratio of signal strength divided by noise standard deviation. The astute reader may be confused by ${\sigma_{\text{ext}}}^{\gamma}$ and σ_{int} having the same units. In future equations we will be more careful; however, this confusing practice is common.

Case 2. If σ_{int} is negligible then we are faced with the problem of Gaussian noise raised to a power making the noise non-Gaussian. Non-Gaussian noise produces a problem in defining d' that is based on Gaussian noise. As long as σ_{int} is negligible, the Gaussian nature of the noise would be restored by raising both sides of Eq. (1) to the $1/\gamma$ power. The new response variable $y^{1/\gamma}$ has Gaussian noise, so it is the appropriate variable for defining d', giving $d' = c_{\text{test}}/\sigma_{\text{ext}}$. This linearization of the dependence on test contrast is Birdsall's theorem. This value of d' is also the value of d' for a generic ideal observer as long as c_{test} and σ_{ext} are defined in terms of the overlap of the stimulus with a template matched to the test pattern, as is discussed following Eq. (2).

Case 3. If neither σ_{int} nor σ_{ext} is negligible, a simple formula for d' isn't possible. This case is the focus of the present paper.

Dosher and Lu [3] and Lu and Dosher [4,5] report their data and data of others where the linearizing effect expected from strong external noise and Birdsall's theorem doesn't hold, and they have developed a model based on multiplicative noise consistent with their finding. In this paper we examine both the experimental and the theoretical underpinnings of the Birdsall linearization effect. Our simulations and our experiments plus data from others show that Birdsall's theorem is more robust than had

 © 2009 Optical Society of America

been expected. We explore how this apparent conflict between different sets of data might be resolved.

We will also consider a related topic of concern to Cohn, called "stochastic resonance," whereby small amounts of noise backgrounds can produce a pedestal effect facilitation similar to that of nonrandom backgrounds [6,7]. Of relevance is Tanner's finding that the presence of uncertainty can mimic a nonlinear transduction. We will argue that uncertainty can serve as an explanation for the stochastic resonance findings and also for violations of Birdsall's linearization by noise.

Although all of our simulations will be based on a discrimination model with multiplicative noise, we will point out that the same conclusions would apply to a class of contrast gain control models with no multiplicative noise. The identity between this broad class of multiplicative noise models and gain control models deflates some of the arguments associated with distinguishing the two [8–11].

Finally, we will thoroughly examine the Perceptual Template Model (PTM) that has the potential for describing both the detection of signals on known pedestals and on unknown noise [3–5]. We modify that model slightly to improve its performance on known pedestals.

2. METHODS

The following simple, plausible, stochastic (inclusion of trial-by-trial noise) model for the response of the visual system to a test pattern is the PTM used by Dosher and Lu [3] (Appendix A):

$$y(c_{\text{test}},\sigma_{\text{ext}}) = (c_{\text{test}}/T_{\text{test}} + \sigma_{\text{ext}}/T_{\text{ext}}\mathbf{R}_1)^{\gamma} + \sigma_{\text{add}}\mathbf{R}_2 + \sigma_{\text{mult}}\mathbf{R}_3, \tag{2}$$

where c_{test} is the overlap of a template with the original noisy stimulus and σ_{ext} is the standard deviation of that overlap with multiple samples of the external noise. We use the notation $\mathbf{R}_i$ as in Eq. (1) for different random numbers on each trial [12]. The first term in Eq. (2) is the output of a single channel that gets stimulation from the test stimulus plus the external random noise, followed by a nonlinear transduction. The last two terms are additive noise following the nonlinearity with the second term ($\sigma_{\text{add}}\mathbf{R}_2$) being a fixed additive noise and the final term ($\sigma_{\text{mult}}\mathbf{R}_3$) being a noise contribution whose strength depends on the stimulus strength of the first term. Because $\mathbf{R}_i$ can be negative and is raised to a power, we define a quantity raised to a power to be $Q^{\gamma}=\text{sign}(Q)\text{abs}(Q)^{\gamma}$ [3].

Before discussing the role of the various parameters, it is useful to specify the performance of the ideal observer specified by $\sigma_{\text{add}}=0$, $\sigma_{\text{mult}}=0$, with the template being matched to the image of the test pattern. The matched filter is the ideal template as long as the noise samples are uncorrelated (white noise). As was derived in Case 2 of the Introduction (Section 1), the d' of the ideal observer is the ratio of the test strength c_{test} divided by the standard deviation of the test strength, σ_{ext}: $d'_{\text{ideal}}=c_{\text{test}}/\sigma_{\text{ext}}$. For this simple formula it is important that both c_{test} and σ_{ext} are measured using a template matched to the test pattern. If the ideal observer is modified by using a template that differs from the ideal template then d' becomes

$$d'_{\text{template}} = (c_{\text{test}}/T_{\text{test}})/(\sigma_{\text{ext}}/T_{\text{ext}}). \tag{3}$$

Levi and Klein [12] called this near-ideal observer the "Template Observer" with the nonideal template able to be estimated using classification images [13,14]. Using both multipass and classification-image techniques we also showed that the mismatched template accounted for almost all of the noise that was consistent across repeated trials. It is useful to note that the conditions for Eq. (3), with the external input noise dominating other sources of noise, are precisely the conditions needed for Birdsall's theorem to produce a linear d' function.

For realistic models the additive and multiplicative noise standard deviations are given in Eq. (2) by σ_{add} and σ_{mult}. y_i (Eq. (2)) can be multiplied by an arbitrary constant without changing d', because d', the measure of psychophysical performance, is based on a ratio of the signal term and the noise terms. We will follow the conventional choice for scaling the parameters by dividing Eq. (2) by σ_{add} [15] and redefining the various parameters so Eq. (2) becomes

$$y(c_{\text{test},1},\sigma_{\text{ext}}) = (c_{\text{test},1}/T_{\text{test}} + \sigma_{\text{ext}}/T_{\text{ext}}\mathbf{R}_1)^{\gamma} + \mathbf{R}_2 + \sigma_{\text{mult}}\mathbf{R}_3. \tag{4}$$

A subscript, 1, has been added to c_{test} for later use to represent one of the intervals of a two-alternative forced-choice (2AFC) experiment. Each term of Eq. (4) is unitless, simplifying its interpretation.

The same formalism can be applied to tasks other than contrast detection or contrast discrimination (like orientation discrimination) by having the single template be the difference of the two stimuli being discriminated. By focusing on the output of a single template, Lu and Dosher simplified the specification of the model while still having it apply to a wide range of tasks [4].

The variables T_{test} and T_{ext} are model parameters that are used in data fitting, and σ_{mult} that specifies the multiplicative noise will be clarified in Eq. (5). T_{test} and T_{ext} play the same role as the Lu and Dosher [4] parameters $1/\beta$ and $1/\alpha$, respectively (see Dosher and Lu [3] p. 1287 for a discussion of their α parameter). Although Eq. (2) is identical to the stochastic version of Lu and Dosher's PTM, we have chosen to slightly modify their notation because their parameters, such as β, are for the analytic version of their model after taking expectation values of Eq. (2) that introduces different relative scaling factors. It is useful to keep the stochastic and analytic versions of the PTM separate, by using separate parameters.

There is some freedom in choosing how the amount of multiplicative noise (σ_{mult}) depends on the test stimulus and the external noise. In order for the TvN (test threshold vs. external noise) curve to have the experimentally found unity log–log slope, the multiplicative noise dependence on external noise needs to have the same power exponent, γ, as the nonlinearity in Eq. (4). For the TvC (test threshold vs. test pedestal contrast) curve the situation is slightly different. The TvC curve typically has a less-than-unity slope [16,17], so the multiplicative noise dependence on the pedestal contrast needs to have a slightly

lower power exponent, γ_t, where $\gamma-\gamma_t$ is the deviation from a unity log–log slope [see the derivation following Eq. (10)]. The multiplicative noise strength σ_{mult} in Eq. (4) can therefore be written as

$$\sigma_{\text{mult}}{}^2 = M_{\text{test}}{}^2(c_{\text{test}}/T_{\text{test}})^{2\gamma_t} + M_{\text{ext}}{}^2(\sigma_{\text{ext}}/T_{\text{ext}})^{2\gamma}. \quad (5)$$

We have replaced the Lu and Dosher multiplicative noise parameters N_{mul} and β_2 with M_{test} and M_{ext} partly to avoid confusing this stochastic model with the PTM analytic model and partly to cleanly separate the test and external noise contributions of the multiplicative noise. In the PTM, the exponent, γ_t would have been chosen to be equal to γ. However, just as Lu and Dosher [5] allowed the coefficients corresponding to M_{test} and M_{ext} to differ, allowing the exponents to also differ is easily accommodated into the PTM, and we will show that pinning down that extra parameter is not a burden for the data fitting. Note that we have omitted the interval-dependent subscript on c_{test} in Eq. (5) that was present in Eq. (4) because the value of σ_{mult} depends on the history of prior stimuli rather than on the trial-by-trial value of c_{test}, so an average of c_{test} values is used in Eq. (5).

Equation (5) brings up a most interesting and troubling question: What is the mechanism that takes the single channel input and breaks it into a pair of branches generating different amounts of multiplicative noise? Two hypotheses can be considered.

Hypothesis 1 is that there is more than one channel from the beginning, each with its own nonlinearity. Given the wide array of spatial frequency channels, it seems arbitrary to have reduced them to a single channel with a single nonlinearity. In fact, multiple channels are needed for the uncertainty explanation of our results (see Section 6, Discussion), so this is the approach we will consider when we discuss uncertainty as an explanation of the data.

Hypothesis 2 is that there is a single input channel [the first term of Eq. (4)] with two multiplicative noise branches [Eq. (5)]. One can now ask the following: What is the characteristic of the stimulus that controls which aspect of the stimulus is the test and which is the external noise channel? Smith and Swift [16] in an article titled "Spatial frequency masking and Birdsall's theorem" argue that the branching has to do with the distinction of which aspect of the stimulus corresponds to an identification task (the Weber, "noise" branch with exponent, γ) and which corresponds to a detection task (the power law, test pattern branch with exponent γ_t for simpler backgrounds). Their experiments show that it is possible for noise patterns to behave as the test branch both by using a simultaneous 3AFC method or by having a lot of practice with the observers becoming very familiar with the noise patterns. The connection between TvN/TvC exponents and the detection/identification distinction will be revisited in the Discussion (Section 6).

All the simulations of this paper will be based on a 2AFC method. The internal response to the interval with the test pattern was given in Eq. (4), and the response to the interval with the reference is

$$y_2(c_{\text{test},2},\sigma_{\text{ext}}) = (c_{\text{test},2}/T_{\text{test}} + \sigma_{\text{ext}}/T_{\text{ext}}\mathbf{R}_4)^{\gamma} + \mathbf{R}_5 + \sigma_{\text{mult}}\mathbf{R}_6. \quad (6)$$

For a detection task, $c_{\text{test},2}=0$. The standard understanding for how 2AFC decisions are made is given by this simple rule:

$$\text{choose interval 1 if } y_1 > y_2, \text{ otherwise choose interval 2.} \quad (7)$$

This simple rule is what allows us to do the nonlinear transformation that was used for obtaining the ideal observer prediction [see Case 2 of the Introduction (Section 1) and Eq. (13)], where all that is required is that the nonlinearity in Eqs. (4) and (6) be monotonic. From Eq. (7) one calculates the probability, p, of guessing the correct interval by dividing the number of correct guesses by the total number (see the Matlab program in Appendix A). p can then be converted to 2AFC d' by using the Matlab erfinv function (see Appendix A): $d'=\text{sqrt}(2)z=\text{erfinv}(2*p-1)*2$. In our discussion comparing the stochastic and the analytic methods we will show using receiver operating characteristics (ROC) curves that the same results are found using a yes/no paradigm as well as a 2AFC paradigm. All that is needed for the yes/no paradigm is to replace y_2 with one fixed criterion (or multiple criteria for rating responses).

Although we will be using the multiplicative noise framework of Lu and Dosher's PTM, all of our simulations and conclusions also apply to a broad class of gain control models, whose structure is mathematically identical to Eqs. (4) and (6). To see that, we first combine the last two additive internal noise terms of Eq. (4) to a single term, $\sigma_{\text{tot}}\mathbf{R}_2$, with

$$\sigma_{\text{tot}} = (1 + \sigma_{\text{mult}}{}^2)^{1/2}. \quad (8)$$

If we now divide Eq. (4) by σ_{tot}, Eq. (4) becomes a gain control model:

$$y(c_{\text{test}},\sigma_{\text{ext}}) = (c_{\text{test}}/T_{\text{test}} + \sigma_{\text{ext}}/T_{\text{ext}}\mathbf{R}_1)^{\gamma}/\sigma_{\text{tot}} + \mathbf{R}_2. \quad (9)$$

The numerator of Eq. (9) is the same as before (omitting the index 1 or 2 for simplicity). The denominator is now the divisive gain control factor. It could be a more general function than that specified by Eqs. (5) and (8) just as the numerator could have been a more complex transducer function rather than a simple power function. What makes this particular gain control model special is the same assumption that makes the PTM multiplicative noise model special: Namely, Eq. (5) that specifies the amount of multiplicative noise [and thus σ_{tot} in Eq. (8)] does not depend on the particular stimulus for a given trial. Rather, it is a time average of previous stimuli. This is an important assumption that is an essential part of the Lu and Dosher PTM. The assumption is reasonable and is in agreement with prior use of the meaning of multiplicative noise [9] as including changes in the subject's state such as caused by adaptation to prior stimuli. We point out this extension to gain control models (no multiplicative noise) because all of our stimulations and discussion apply equally well to that broad class of models. The gain control models of Eq. (9) are barely distinguishable from the gain control models of past studies [7,17,18]. The

appendix of Legge *et al.* [19] presents a derivation connecting a compressive nonlinearity model to the multiplicative noise model. Their derivation does not consider the complication of how to deal with the non-Gaussian noise distribution following the nonlinearity. Although we too avoid that complication [but see our discussion in connection with Figs. 4(d) and 4(e)], our derivation above shows that the two models we consider are identical.

We now turn our attention to how to estimate the six model parameters: γ, γ_t, T_{test}, M_{test}, T_{ext}, and M_{ext}. The first four parameters can be determined just from the data with no external noise ($\sigma_{\text{ext}}=0$). The last two can be pinned down from a combination of the high external noise thresholds plus the double pass % agreement that will be examined in connection with the simulations. For the first four parameters, simulations are not needed since for $\sigma_{\text{ext}}=0$ the signal and its standard deviation in Eqs. (4) and (5) simplify, giving, with *no approximations*, an *analytic* expression for d':

$$d' = (c_{\text{test}}/T_{\text{test}})^{\gamma}/(1 + M_{\text{test}}{}^2(c_{\text{test}}/T_{\text{test}})^{2\gamma_t})^{1/2}. \quad (10)$$

The denominator of Eq. (10) is barely different from the d' formula proposed in Eq. (3) of Stromeyer and Klein [19] that has the form $d'=c_{\text{test}}{}^{\gamma}/(a+bc_{\text{test}}{}^{\gamma_t})$ and is commonly used for fitting TvC functions [17,20]. Equation (10) allows one to estimate T_{test}, M_{test}, γ, and γ_t. The behavior at low values of c_{test} enables estimation of T_{test} and γ since the denominator ≈ 1. At high values of c_{test} the asymptotic form of Eq. (10) is $d' \approx c^g/M_{\text{test}}$, where $g=\gamma-\gamma_t$ and $c=c_{\text{test}}/T_{\text{test}}$. Threshold for contrast discrimination is defined to be the contrast change needed to give $\Delta d'=1=g/M_{\text{test}}c^{g-1}\ \Delta c$, so $\Delta c=c^{1-g}M_{\text{test}}/g$. If the asymptotic d' function has a log–log slope of $g=0.3$, then the discrimination TvC curve will have a slope of $1-g=0.7$, slightly shallower than the TvN function that has unity slope. The parameter M_{test} in Eq. (10) corresponds to the point at which the TvC curve begins to saturate near the trough of the TvC dipper function. These relationships correspond to the most standard approach to dealing with contrast discrimination [8,9] because at high pedestal contrasts the contrast discrimination TvC curve is well fitted by a power function. The basic assumption underlying our approach using the ambitious PTM is that a single model is able to fit the TvC curve for $\sigma_{\text{ext}}=0$, as well as the TvN curve for $\sigma_{\text{ext}}>0$. Our point here is that most [Eq. (4)] of the PTM parameters can be well estimated in the $\sigma_{\text{ext}}=0$ regime.

Pinning down the last two parameters, T_{ext} and M_{ext}, from experimental data is more subtle than measuring the first four. If classification images had been measured, then in the Dosher and Lu [3] stochastic framework it would be possible to pin down T_{ext}, in which case M_{ext} could be determined by the height of the TvN curve. However, without classification images the parameters T_{ext} and M_{ext} are totally correlated [see Eq. (23)]. Thus, in order to disambiguate T_{ext} and M_{ext}, Lu and Dosher [5] must use both the TvN curve and also the double-pass information. The larger the value of M_{ext} (more additive noise) for a given T_{ext}, the smaller will be the double-pass % agreement. We will clarify this claim in connection with our simulations, to be discussed next. Levi *et al.* [14] consider the consequence of having additional classification-image constraints for pinning down parameters.

3. PARAMETERS FOR SIMULATIONS

The simulations are surprisingly simple to do and just amount to writing down Eqs. (4)–(7) in Matlab and then plotting the results. The full program for the calculations going into Figs. 1 and 3 (Fig. 2 is from human data) is presented in Appendix A. We start by discussing how the six parameters of the model were chosen for the simulations.

The two parameters T_{test} and T_{ext} are merely scaling parameters for the abscissa and ordinate of the TvN curve to be shown as the second column of panels in Fig. 1. That their only role is scaling the test contrast and the external noise contrast can be seen in Eqs. (4)–(6), where the only appearance of c_{test} and T_{test} is in the combination $c_{\text{test}}/T_{\text{test}}$ and the only appearance of σ_{ext} and T_{ext} is in the combination $\sigma_{\text{ext}}/T_{\text{ext}}$. For example, by doubling T_{test} all TvN curves shift rightward by a factor of 2. In fitting real data, T_{test} would be very close to the detection threshold of the test pattern when $\sigma_{\text{ext}}=0$ [see Eq. (20) for the exact relationship]. Given this flexibility in defining T_{ext}, we arbitrarily choose a value of $T_{\text{ext}}=1$ for our simulations. In our simulations we fix $T_{\text{test}}=1.25$. Figure 2 of Levi *et al.* [14] shows that based on their classification images the nonamblyopic eye of amblyopic observers as well as of normal observers had $T_{\text{test}} \approx 1.25$ [note T_{test} is the reciprocal of the square root of efficiency as shown in Fig. 2 of Levi *et al.* [14] and as noted in connection with our Eq. (3)]. Several of the amblyopic eyes of the amblyopes had T_{test} as high as 2.0. This small vertical TvN shift due to $T_{\text{test}}>1$ is pointed out in the top panel of Fig. 1(b). We have arbitrarily chosen $T_{\text{ext}}=1$ since this is the default choice of the Dosher and Lu PTM [3]. That is, they tend to normalize Eq. (2) by dividing both sides by T_{ext}, whereas we tend to normalize it by dividing both sides of Eq. (2) by σ_{add} to obtain Eq. (4). When fitting real data, the value of T_{ext} is tightly correlated with the value of M_{ext} so the two of them must be fit together, a topic to be explored in our simulations and Discussion (Section 6).

For the exponent, γ, specifying the low-contrast d' (transducer) function exponent, Lu and Dosher [5] report values between 2.05 and 2.36 in their Table 4. For simplicity, we fix it at $\gamma=2$ for the simulations. This is the exponent that characterizes the numerator of the d' function in Eq. (10). As was discussed following Eq. (10), the exponent γ_t can be obtained by looking at the asymptotic slope of the TvC function that is specified by $1-(\gamma-\gamma_t)$. It is found to have slopes ranging from 0.5 to 0.8 [17,16,20]. For our simulations we take the log–log TvC to be 0.7 so that the asymptotic d' slope is 0.3, giving a value of $\gamma_t=\gamma-0.3=1.7$. The Lu and Dosher [5] choice would have had $\gamma_t=\gamma=2$ corresponding to an implausible ceiling of the d' function with a hard saturation at $d'=1/M_{\text{test}}$.

For our simulations we have chosen three sets of multiplicative noise parameters corresponding to the three rows of Figs. 1 and 3: $[M_{\text{test}},M_{\text{ext}}]=[0,0]$, [0.33, 1.5], and [0.33, 5]. The first pair corresponding to zero multiplicative noise is a baseline simulation. The specific value of $M_{\text{test}}=0.33$ was chosen because, as will be discussed

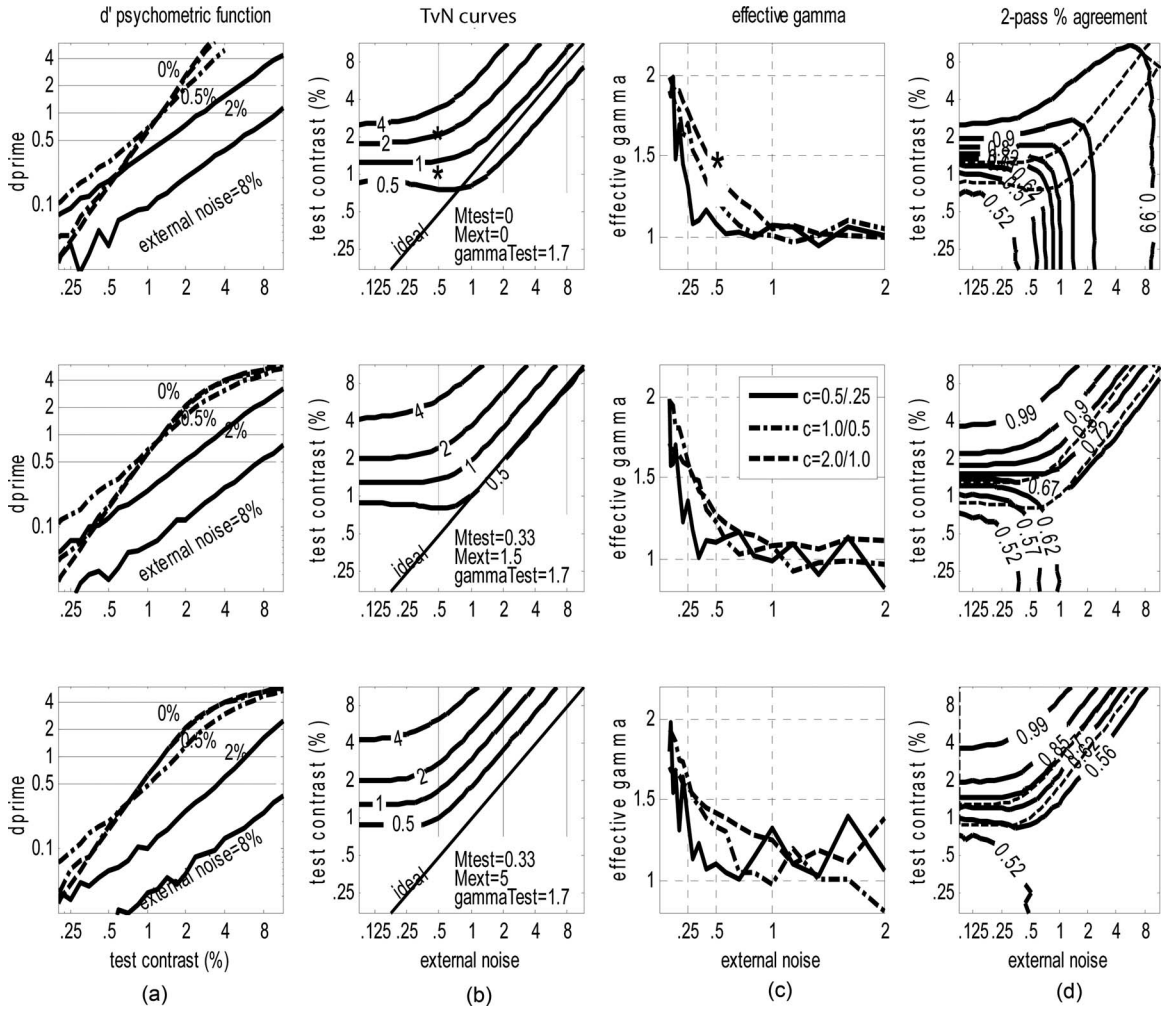

Fig. 1. Result of simulations of the perceptual template model specified by Eqs. (4)–(7). The model parameters are $\gamma=2$, $\gamma_t=1.7$, and $T_{ext}=1$ and $T_{test}=1.25$. The values for the M_{ext} and M_{test} vary for the three rows of the figure as indicated in the legends in the three (b) panels. (a) is a plot of d' vs. test strength for four strengths of external noise, 0, 0.5%, 2%, and 8%. The d' curve for zero external noise [from Eq. (10)] is much steeper than those for the simulations with substantial external noise (Birdsall linearization). (b) is from the same data as (a) but replotted as TvN curves (test contrast vs. external noise strength) for d' levels of 0.5, 1, 2, and 4, corresponding to the four horizontal lines in (a). The three vertical lines in (b) correspond to the three nonzero values of external noise in (a). (c) shows the effective exponents of d' psychometric functions. They correspond to the slopes of the log–log curves in (a). (d) has the same abscissa and ordinate as (b), but the contour lines are now iso % agreement showing the fraction of times the observer gives the identical response in a 2AFC method to trials with identical external noise. The dashed lines are replotted from (b) for $d'=0.5$ and 1.0.

following Eq. (18), the Lu and Dosher fit for M_{test} in their Table 4 for their three observers were $M_{test}=0.33,0.30,0.35$ [5]. These are very reasonable values in that they correspond to having the d' saturation begin slightly above the detection threshold, as we have found in our contrast discrimination studies without external noise. We also explored broad ranges of other values for M_{test} and reasonable values for γ_t and found that the results of the simulations were similar, showing strong Birdsall linearization. The value of $M_{ext}=1.5$ was chosen because it is a reasonable upper limit to the data ($M_{ext}=[1.23,0.70,$ and $1.60]$) of the three observers in Table 4 of Lu and Dosher [5]. As will be discussed, the data that place a strong constraint on these values for M_{ext} come from the % agreement of the double-pass data shown in Fig. 19 of Lu and Dosher [5]. Finally, we also carried out simulations for $M_{ext}=5.0$, a level more than 3 times above the most reasonable level. We do this to demonstrate that even with this extra large amount of multiplicative noise we still find strong Birdsall linearization.

4. SIMULATIONS

The Matlab code for our simulations is given in Appendix A. Our simulations are done by carrying out Eqs. (4)–(7), 50,000 times.

The results of simulations of Eqs. (4)–(7) are shown in Fig. 1 for the parameters discussed above and for a "continuum" of stimulus values c_{test} and σ_{ext} whose range is visible as the abscissa and ordinate of the plots in the second column of Fig. 1 [Fig. 1(b)].

The three rows of panels are for multiplicative noise values of $[M_{test}M_{ext}]=[0,0]$, [0.33, 1.5] and [0.33, 5.0]. Figure 1(a) (the leftmost panels) presents the raw plots of d' for detection ($c_{test,2}=0$) as a function of c_{test} for $\sigma_{ext}=0$, 0.5, 2, and 8. These plots are often called transducer func-

tions. We prefer to call them d' psychometric functions since d' is directly related to the 2AFC probability correct and since complexities associated with multiplicative noise or stimulus uncertainty or gain control distort their shape from what goes on at the early transduction stage.

The case $\sigma_{ext}=0$ in the three panels of Fig. 1(a) are shown as a dashed curve, given by Eq. (10) to be

$$d' = (c_{test}/1.25)^{\gamma}/(1 + M_{test}{}^2(c_{test}/1.25)^{2\gamma_t})^{1/2}, \quad (11)$$

where $\gamma=2$ and $\gamma_t=1.7$ as discussed above. In the upper panel of Fig. 1(a) ($M_{test}=0$), this dashed curve ($\sigma_{ext}=0$) is given by $d'=(c_{test}/1.25)^{\gamma}$ so on the log–log axes it is a straight line of slope $\gamma=2$. The lower two panels of Fig. 1(a) show the dramatic change in slope of the d' function as external noise is added. The third column of panels [Fig. 1(c)] give the effective $\gamma(\gamma_{eff})$ of the simulations, and it is seen that γ_{eff} is indeed equal to 2 for zero external noise. In order to show how γ_{eff} was calculated, an asterisk is placed on one of the points in the upper panel of Fig. 1(c). The three curves in Fig. 1(c) are for three ranges of test contrast used for calculating the effective slope. The formula used for γ_{eff} is based on the assumption that locally $d'(c)\approx kc^{\gamma_{eff}}$. Thus $d'(c)/d'(c/2)=c^{\gamma_{eff}}/(c/2)^{\gamma_{eff}}=2^{\gamma_{eff}}$, and

$$\gamma_{eff}(c_{test}) = \log(d'(c_{test})/d'(c_{test}/2))/\log(2), \quad (12)$$

where d' is shown in panels 1(a) and 1(b) from the simulations. This is the log–log slope of the d' function. The point with the asterisk is for $\sigma_{ext}=0.5$ and $c_{test}=2$ [the dashed curve in Fig. 1(c)]. Asterisks are also placed on the corresponding points for $\sigma_{ext}=0.5$ and $c_{test}=1$ and 2 in the upper panel of Fig. 1(b) to provide further clarification of how γ_{eff} was calculated.

When a slight amount of external noise is introduced, something unusual occurs as seen in the dotted–dashed curves for $\sigma_{ext}=0.5$ of Fig. 1(a). The psychometric function has become shallower than the $\sigma_{ext}=0$ plot, pivoting around a point below $d'=1$. By the time the external noise reaches $\sigma_{ext}=1$, the log–log slope has fallen to unity as shown in Fig. 1(c), where γ_{eff} reaches its asymptotic level quite rapidly. This dramatic linearization of the d' psychometric function is a consequence of Birdsall's theorem. One fascinating consequence of the pivoting is that for test contrasts below the pivot point, d' actually *increased* due to the presence of external noise. This facilitation phenomenon has been called stochastic resonance by the physics community. As will be clarified in the Discussion (Subsection 6.D), it is quite possible that the facilitation by noise is due to uncertainty reduction rather than by the nonlinear model of Eq. (4). Uncertainty is the competing explanation for both the linearization of the TvC (disappearance of the dipper at high noise levels) and the facilitation (stochastic resonance at low noise levels) as will be clarified in Subsection 6.D.

Figure 1(b) is the same data as Fig. 1(a) but plotted differently (see Appendix A) and for a continuum of values of σ_{ext}. Figure 1(b) plots the values of c_{test} that are needed to give d' values of 0.5, 1, 2, and 4. Note that the values for the levels were chosen to be equally spaced on log–log coordinates. These d' levels are indicated in Fig. 1(a) by the horizontal lines, just as the external noise levels of Fig. 1(a) are indicated in Fig. 1(b) by the three vertical lines. The plots in Fig. 1(b) are the commonly used threshold vs. noise, TvN, plots. As seen in the Matlab program of Appendix A, the TvN plots of Fig. 1(b) are simply produced by Matlab's "contour" function.

Birdsall's theorem is "evident" in these Fig. 1(b) plots as we note that the TvN curves for $d'=0.5$ and 1 are closer together for $\sigma_{ext}<1$ than for $\sigma_{ext}>1$. Quotes have been placed around the word (evident) because it isn't perceptually evident. One must use a ruler to convince oneself because of an illusion that the tilted lines at 45 deg appear closer together than their vertical separation indicates. Surprisingly, this illusion was also present in a demonstration of Birdsall linearization in Fig. A1 of the appendix of Dosher and Lu [3] that shows results from the stochastic PTM! Again a ruler is needed to see the stunning Birdsall effect. The analytic version of the PTM model is not in accord with these simulations since it predicts a constant vertical shift of the TvN curves (log axes) for different d' values [see Eq. (19) of Section 6]. The Birdsall effect is diminished for the $c_{test}=2.0$ to $c_{test}=1.0$ comparison because for $c_{test}=2$ the nonlinear saturation has already begun to linearize the TvC function even in the absence of external noise. Thus to see the Birdsall mechanism one needs to look at low d' levels.

Also shown in Fig. 1(b) is a straight line representing the ideal observer prediction for $\sigma_{add}=\sigma_{mult}=0$ (no internal noise). As was discussed for Case 2 in the Introduction (Section 1) and in the discussion leading to Eq. (3), the ideal observer's performance is given by

$$d'_{ideal} = c_{test}/\sigma_{ext}. \quad (13)$$

The detection or discrimination threshold for the ideal observer plotted in Fig. 1(b) is given by $c_{test}=\sigma_{ext}$ since threshold is defined to be at $d'=1$.

Also present in Fig. 1(b) is a small stochastic resonance facilitation that is produced by the external noise. The amount of the dip is less than what is seen in Fig. 1(a) near $d'=0.1$ because the dip appears only for very low values of d'. It is gone by $d'=1$. In Fig. 1(b) the dip is for the curve with $d'=0.5$, corresponding to the lowest of the horizontal lines in Fig. 1(a). If we had plotted the case of $d'=0.1$, a deeper dip (on log axes) would have been found, but the percent error of the curves make measurements at such low values of d' impractical.

As pointed out following Eq. (10), the data for the d' psychometric function for the zero external noise case ($\sigma_{ext}=0$) can determine T_{test}, M_{test}, γ and γ_t. Left undetermined in Eqs. (4) and (5) are T_{ext} and M_{ext}. Unfortunately these two parameters are highly correlated and the data is sufficiently noisy that they are not able to be accurately pinned down based on the discrimination data shown in Figs. 1(a)–1(c), This is because all the TvN curves of Fig 1(b) can be shifted right or left either by multiplicative noise or by the unknown sensitivity of the template to the noise, T_{ext}. This ambiguity is especially apparent in the analytic version of the PTM as will be explicitly shown in Eqs. (22) and (23). Lu and Dosher realized this problem, so they made use of the double-pass method for estimating the amount of multiplicative noise [5]. The ambiguity can also be resolved using classification images, as is discussed in Levi *et al.* [14]. By combining both classification

images and the double-pass method one has the ability to detect additional sources of double-pass consistency not captured by the classification-image template.

The double-pass method repeats trials using the same Eqs. (4) and (6) values for $c_{test,1}$, $c_{test,2}$, σ_{test}, $\mathbf{R}_1$ and $\mathbf{R}_4$ and with the additive and multiplicative noise free to vary in the second pass [21]. One then calculates the percent of responses that are in agreement in the repeated trials (the line *agree=mean(w2==w1)*, in the Matlab program in Appendix A). Figure 1(d) is a contour plot with the same axes as Fig. 1(b), but now the contour lines are the double-pass % agreement. Figure 1(d) shows that these contour lines are sensitive to the amount of multiplicative noise. The double-pass data together with the location of the TvN curves at large values of noise are able to pin down T_{ext} and M_{ext}, the two parameters not determined by the $\sigma_{ext}=0$ data discussed above. The plots of Fig. 1(d) are a complement to the more common Burgess-type plots of % correct vs. % agreement that will be discussed in the next section. The two dashed curves in Fig. 1(d) are the $d'=0.5$ and 1.0 curves from Fig. 1(b). They are presented to show a region where the double-pass constraint can restrict parameters effectively.

5. RESULTS OF EXPERIMENTS

Figure 2 summarizes our experiments, averaged over five normal observers and representing in excess of 40,000 trials on contrast detection of a Gabor, bar-like pattern in one-dimensional noise. Details of the stimuli and methods are given in Levi *et al.* [14]. However, here we emphasize that particular attention was given to minimizing uncertainty in the experiments. Specifically, the stimulus was a highly localized bar-like pattern with fixed phase and a position that was clearly marked by a fixation line adjacent to the target. Without that fixation line there would surely have been position uncertainty of the test pattern. Second, it was presented with a long duration (0.75 s), and the onset was clearly marked by a tone, minimizing temporal uncertainty. Third, for each noise level, performance was measured using the method of constant stimuli (four signal contrasts including a blank) that enabled us to measure d' at three contrast levels. Finally, data were collected in runs of 410 trials, preceded by 20 practice trials. Each condition (identical signals and noise) was performed three or four times in separate runs (1230–1630 trials), before moving to the next condition.

The format of Fig. 2(a) is the same as that of Fig. 1(a), and Fig. 2(b) is the same as that of Fig. 1(c). The abscissa of Fig. 2(a) is the peak contrast of the Gabor test patch, and the ordinate is the d'. The five sets of data, coded by symbol size, are for five noise strengths of 0, 2, 5, 10, and 20 NTU (noise threshold units), and 5 NTU means a noise strength 5 times the noise detection threshold. The noise detection threshold was measure separately. The noise detection threshold has special relevance to TvN plots such as those shown in Fig. 1(b) because Levi *et al.* [13,14] showed that the noise detection threshold is typically very close to the equivalent input noise, N_{eq}, that is the kink point in the TvN curves. Equation (23) expresses N_{eq} in terms of T_{ext} and M_{ext}.

On log–log axes the d' vs. test contrast plot for each

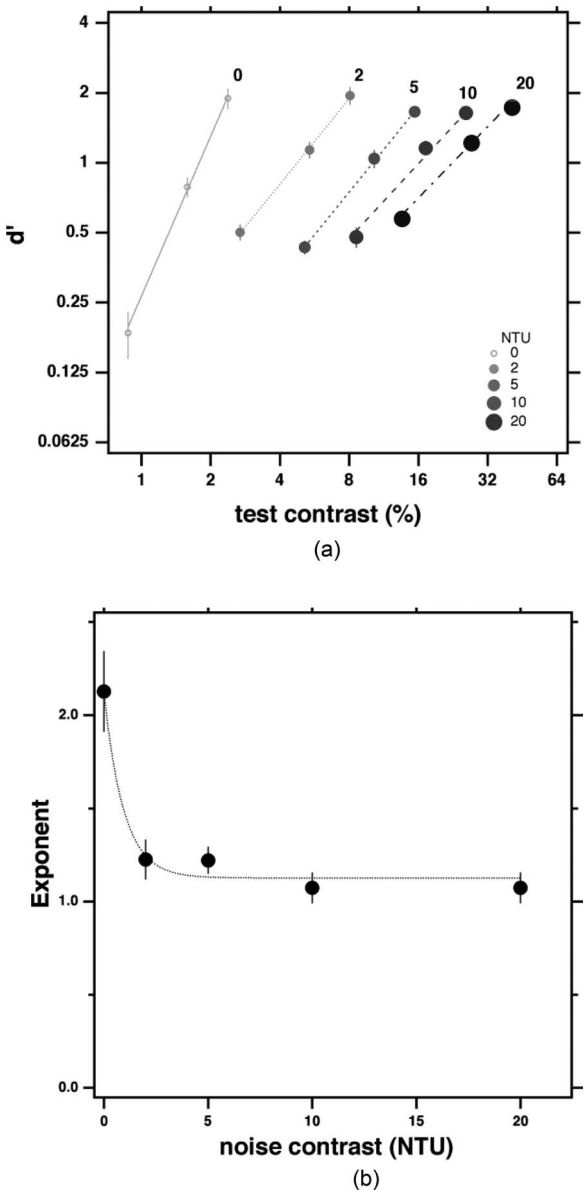

Fig. 2. Reanalysis of the data of Fig. 15 of Levi *et al.* [14] for five normal observers. (a) is similar to Fig. 1(a), except that the external noise is specified in noise threshold units (NTU) (see the numbers above the data). NTU=2 means the noise was twice its detection threshold at $d'=1$. The abscissa and ordinate show that logarithmic axes are being used. (b) is the effective exponent of the d' function and is given by the log–log slope of the data in (a). There is a dramatic reduction of the slope once external noise is present, as would be suggested by Birdsall's theorem.

noise strength falls remarkably close to being on a straight line (power functions fitted to the data). The log–log slopes of these lines are shown in Fig. 2(b), where the abscissa is in NTU and the ordinate is the effective exponent, γ_{eff}, of the d' psychometric function. The plot shown in Fig. 2(b) with a rapid decay to $\gamma_{eff}=1$, is well matched to the results of the stochastic PTM model shown in Fig. 1(c). However, as will be noted in the Discussion (Section 6), there are also experiments, including that of Lu and Dosher [5] where the d' exponent in moderate and high external noise is barely different from the exponent at zero external noise. Uncertainty reduction models will be

considered as a possible explanation for the apparent violation of Birdsall's theorem in those experiments.

It is important for our Birdsall theorem argument in the context of the PTM to place limits on the amount of multiplicative noise. If it is much larger than the postnonlinearity external input noise, then the assumptions underlying Birdsall's theorem wouldn't hold. Data that is relevant to this question come from Fig. 2 of the Levi *et al.* [14] study that shows the square root of detection efficiency of the data in our Fig. 2. For the normal observers the human to ideal threshold ratio is about $1/0.55=1.82$ and the template to ideal threshold ratio is about $1/0.8=1.25$. Thus the human-to-template ratio is about $0.8/0.55\approx1.45$. As discussed at the beginning of Section 3, we have fixed the parameters of all of our simulations to have $T_{test}/T_{ext}=1.25$, to be in agreement with the template inefficiency that is found in normal observers. This choice can be validated by inspection of the top panel of Fig. 1(b), where the $d'=1$ TvN curve is elevated above the ideal observer prediction by a factor of about 1.25. The $d'=1$ TvN curve in the middle panel of Fig. 1(b) is almost a factor of 2 above the ideal observer prediction, compatible with the factor of 1.82 for the Levi *et al.* (Fig. 2) [14] normal observers mentioned above. This middle panel with the multiplicative noise parameter of $M_{ext}=1.5$ matches the human data estimate calculated above of 1.45 very well. As seen in the middle panel of Fig. 1(c), this amount of multiplicative noise still has a dramatic Birdsall theorem decline in the effective exponent. The bottom panels of Fig. 1 are for the case of more than triple ($M_{ext}=5$) the amount of multiplicative noise exhibited by our human observers. Yet the effect of Birdsall's theorem is still present and especially visible at low d'. Our Eq. (18) provides further evidence that our value of $M_{ext}=1.5$ is near the upper limit of the experimental values found by Lu and Dosher [5].

Further validation that the amount of multiplicative noise must be relatively small is provided by the multipass agreement data in Fig. 16 of Levi *et al.* [14]. Across the entire range of spatial frequencies the ratio of random noise power to total noise power is between 0.4 and 0.6 for the normal observers. This is for data with substantial external noise, so the internal noise is negligible and the random noise is entirely multiplicative noise. Thus the threshold elevation due to the random noise is a factor of sqrt(2) larger than the consistent noise (the sqrt is because Fig 16 is for power rather than contrast). This factor is compatible with the factor of $0.8/0.55=1.45$. As mentioned above in connection with threshold elevation, this amount of multiplicative noise matches that found in our simulations for the multiplicative noise being $M_{ext}=1.5$.

A. Double-Pass Data of Lu and Dosher and the Burgess Plots

Figure 19 of Lu and Dosher [5] presents double-pass data from their three observers plotted in a Burgess-style plot of % correct vs. % agreement for a 2AFC method [21]. In order to make contact with their data, in Fig. 3 we replot our Fig. 1(c) in the more common Burgess format. Before getting to the Lu & Dosher data [5] (Fig. 19) we discuss several enhancements to the usual Burgess plots that are made in Fig. 3.

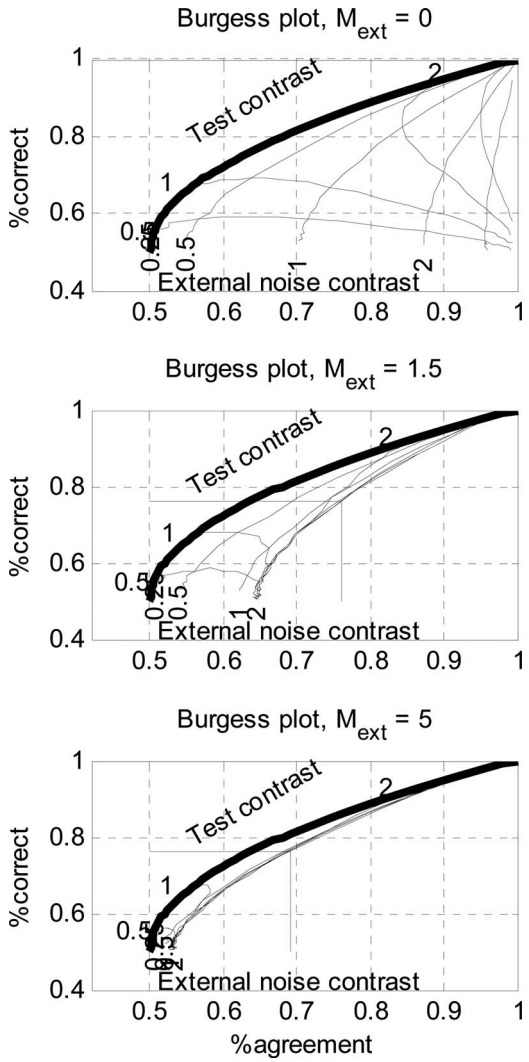

Fig. 3. The double-pass % agreement data from Fig. 1(c) is replotted "inside-out" with axes following the Burgess and Colborne [21] diagram. The three panels have the same parameters as Fig. 1. The axes are the % agreement and % correct with contour lines being strength of test pattern and external noise. The leftmost parabola is independent of model parameters and represents the limiting case where the probability of a correct judgment does not depend on the particular external noise being shown. It is seen that as the external noise increases, the % agreement also increases. Also shown are lines of constant signal strength of $c_{test}=0.5$, 1.0, and 2 as well as lines of constant external noise. The positive slope at the left portion of the $c_{test}=0.5$ curve shows the stochastic resonance effect. The horizontal line at 76% correct ($d'=1$) shows how the % agreement can distinguish among the three values of $M_{ext}=0$, 1.5, and 5.0 that are shown in the three panels.

One enhancement is an analytic formula for the case of zero external noise ($\sigma_{ext}=0$). This is the leftmost (the minimum) part of the allowable values for p_{agree} that is shown as a thick curve. This case is especially simple because the correlation of responses in the two repeated trials is zero, i.e., if the probability of being correct in the first interval is p, then the probability of being correct in the second interval is also p. Thus the probability of

agreement is the probability of both intervals being correct plus both being incorrect:

$$p_{\text{agree-min}} = p^2 + (1-p)^2 = \tfrac{1}{2} + 2\left(p - \tfrac{1}{2}\right)^2 \quad \text{for } \sigma_{\text{ext}} = 0, \tag{14}$$

and it is seen that the Burgess curve is a simple parabola of $p_{\text{agreement}}$ as a function of the probability correct, p. This analytic curve for $p_{\text{agree-min}}$ is independent of any model parameters. This curve of minimum agreement is the limiting case as the multiplicative noise increases, as can be seen in the three panels where the multiplicative noise increases from $M_{\text{ext}}=0$ to 5.

A second innovation in our plots is that we present a few iso-test strength curves as well as the iso-external noise curves on the plot. The resulting "spiderweb" mesh provides all the information linking % correct and % agreement to the stimulus parameters that had required two plots [Figs. 1(b) and 1(d)] previously. Finally, we make a connection with the $d'=1$ curves that are shown in Figs. 1(b) and 1(c). In Fig. 3, the $d'=1$ curve is simply the horizontal line at $p=76\%$ that corresponds to $d'=1$ for a 2AFC task. We extend the $d'=1$ line to the rightmost portion of the % agreement, corresponding to higher values of the external noise. For increasing amounts of multiplicative noise the % agreement saturates. For $M_{\text{ext}}=1.5$ and 5.0 the saturation is at 76% and 71%, respectively, as seen in the vertical line that intersects the $d'=1$ point.

For all three of observers in Lu and Dosher's Fig. 19 the % agreement is at least 70% correct at $d'=1$ ($p=76\%$), and for observer SJ, p_{agree} is greater than 80% [5]. For SJ this large amount of agreement means $M_{\text{ext}}<1.5$. For the other two subjects $M_{\text{ext}}<3$. Any larger values would have introduced more randomness that would have degraded the % agreement. Yet even for values as large as $M_{\text{ext}}=5$, the bottom panel of Fig. 1(d) shows that Birdsall's theorem holds. The Discussion (Subsection 6.A) will examine another aspect of SJ's interesting results.

B. Departures from the PTM in Amblyopic Vision

The preceding discussion was based on the PTM assumption that before the nonlinearity only the fixed, systematic noise coming from the external noise was present. If, however, the template has trial-to-trial instability [23], as may be expected in the presence of stimulus uncertainty, then a random multiplicative term, whose strength is given by M_{early}, would be present before the nonlinearity, so Eq. (4) becomes

$$y(c_{\text{test},1}, \sigma_{\text{ext}}) = (c_{\text{test},1}/T_{\text{test}} + \sigma_{\text{ext}}/T_{\text{ext}}\mathbf{R}_1 + \sigma_{\text{ext}}M_{\text{early}}\mathbf{R}_m)^{\gamma} + \mathbf{R}_2 + \sigma_{\text{mult}}\mathbf{R}_3. \tag{15}$$

A fluctuating template is multiplicative because the stronger the external noise, the stronger will be the output of the fluctuating template. Evidence for this early nonlinearity may be found in several figures of Levi *et al.* [14] data on amblyopes. Their Fig. 6 shows degraded efficiency in the presence of noise; their Fig. 12 shows decreased % agreement, yet Fig. 16 shows as much linearization as in normal observers. Thus, by departing from the PTM model and by putting some of the multiplicative noise before the nonlinearity, one is able to have arbitrarily large amounts of Birdsall linearization even with arbitrarily large amounts of multiplicative noise. It should be noted that M_{early} isn't an extra parameter since the extra amount of pre-nonlinearity noise could be achieved by a reduction of the previously present parameter, T_{ext}.

If one calls the fluctuating template a case of template uncertainty, then we have the curious situation that uncertainty can either increase or decrease the d' nonlinearity. Template uncertainty, as in Eq. (15), that comes before the nonlinearity will have the effect of linearizing the psychometric function (reducing the dipper facilitation in a contrast discrimination task). However, decision stage uncertainty about which mechanism has the signal will act as an accelerating nonlinearity even at large amounts of external noise. This latter, more standard, definition of uncertainty cannot be put into the single-channel formula such as Eq. (15) because that form of uncertainty requires multiple channels.

In summary, data from human observers show a dramatic drop in the effective exponent of the d' vs. test contrast plot as the external noise increases. This finding is not surprising since the simulations showed that for these same observers the amount of multiplicative noise is sufficiently low ($M_{\text{ext}}<3$) that for the stochastic PTM the external noise provides strong linearization of the d' psychometric function. That is, the dipper is removed. One challenge that needs to be addressed in the Discussion is why are there such a diversity of data with no linearization [4,5,22], modest linearization [15,24], or strong linearization [14,25]?

6. DISCUSSION

A. Experimental Conditions and Uncertainty

Our data in Fig. 2 show that once external noise is introduced, the effective exponent of the d' psychometric function falls dramatically from a value above 2 for zero noise to a value very close to 1, consistent with Birdsall's theorem. However, there is a great mixture of findings on this topic. This is quite perplexing. Why should there be such a diversity of findings? This section will consider the possibility that the diversity of results is due to the diversity of uncertainty across experimental conditions and across observers [26]. But we first examine a representative number of these discordant findings.

The psychometric functions found by Lu and Dosher [4,5] and Dosher and Lu [3] consistently show strongly accelerating functions with similar slopes independent of the amount of noise masking including the no-noise condition. Pelli [22] shows a similar strong dipper function for both with noise and no noise, with the dipper being the sign of a steeply accelerating psychometric function. Many reports, on the other hand, show a mixed finding. Figure 1(a) of Goris *et al.* [15] shows that the no-noise d' function is much steeper than when noise is present. However, full linearization is not achieved, as is seen by the presence of the dipper in their Fig. 1(c), indicating there is still more acceleration of the d' function than we find in our Fig. 2 or than in our Birdsall theorem predictions in Fig. 1. Henning and Wichmann [24] have a mixture of results across subjects, with observer GBH show-

ing a very deep dipper in the no-noise condition. The dipper pretty much disappears in the white-noise condition. On the other hand, observer NAL shows a relatively constant dipper across conditions, while TCC's dipper is between the other two. It is worth pointing out that Henning and Wichmann [24] also had a condition with "notched noise" where the noise background had a noise-free notch, nearly two octaves in width, with the test pattern in the center. This notched noise was the most powerful of all maskers in raising thresholds and also in linearizing the psychometric function. One would hesitate in calling this linearization a Birdsall linearization since an observer with a well-matched template would barely see the noise at all. Their finding provides a wonderful reminder that there is still much to learn about the detection of targets in noise. Happily, Goris, Wichmann, and Henning [27] have more recently developed a quite plausible model based on detailed physiological reasoning that can account for their surprising data.

Since even a small departure from constancy of slope will cause a problem for the analytic version of the PTM, it is useful to look closely at another case of partial linearizing in the Lu and Dosher [5] data for observer SJ. Toward the end of the Results section (Section 5), we pointed out that observer SJ had a substantially larger amount of % agreement than the other two subjects. A larger % agreement could be a sign of less multiplicative noise and/or less uncertainty. Inspection of Fig. 20 of Lu and Dosher [5] shows that indeed the high % agreement is associated with a reduction of the effective d' exponent in going from $\gamma_{\text{eff}} \approx 2.5$ in the no-noise condition to around 1.8 in the presence of noise. This exponent was calculated by comparing the threshold ratios for their top plot for $d'=1.47$ ($p_{\text{correct}}=85\%$) to their bottom plot for $d'=0.54$ ($p_{\text{correct}}=65\%$). Although it may not be significant at the 0.05 level for a slope change, that datuma is worth mentioning because it also shows a stochastic resonance hint of facilitation by the noise, a topic soon to be considered below.

One of the most interesting reports of mixed findings is Kersten's [25] (Table 2) finding in two observers that the detection of low-spatial-frequency bars (0.25 deg in width) on a blank field had slopes of $\gamma=2.34$ and 2.86, and with a dynamic white-noise background the slopes were $\gamma=1.15$ and 1.04. However, for thin bars (0.016 deg in width) on the same dynamic noise, the slopes for the same observers jumped to $\gamma=2.67$ and 2.62! Legge *et al.* (Table 1) [19] replicated the wide bar finding of very strong linearization. These results on how the stimulus can affect slope linearization are compatible with an uncertainty explanation, as we now consider.

We believe that an important contribution to the differences in Birdsall linearization between datasets may be due to differences in uncertainty associated with experimental considerations. In Kersten's experiments there would be much more position uncertainty with the very thin stimuli so any accelerated of the d' function would be found no matter what type of background was present. However, with the wider stimuli, position uncertainty is reduced and the noise mask could well be sufficient to identify which are the responsive neurons worth attending, thereby removing the remaining uncertainty and thereby linearizing the psychometric function. For this reason our stimuli, discussed in connection with Fig. 2, were designed to maximize the visual system's ability to precisely attend to the relevant features of the target. The target was a local one-dimensional Gabor-like grating with approximately two cycles. The location of the peak was carefully identified by short bars at the edge of the stimulus (see the inset of Fig. 1 of Levi *et al.* [14] for more details). The long duration and the presence of one-dimensional external noise should dramatically reduce any uncertainty about the orientation and timing of the test pattern. Lu and Dosher [5], Pelli [22], and Goris *et al.* [28] used very brief stimuli. They also used stimuli with multiple cycles (7 c/deg in the Goris case), producing phase uncertainty. For some of the studies an additional problem is that all noise and test conditions were intermixed. For example in the Goris *et al.* [15] study, three noise powers and ten test pedestal levels were intermixed in a single run. Lu and Dosher typically intermixed different noise levels (also see Experiment 2 of Goris *et al.* [28]). Randomizing the noise levels may result in observers using different neuronal populations on some trials than on others (for example when the noise is weak vs. strong). Even without intermixing conditions, the two-dimensional white noise that is typically used provides no cues to the observer as to which oriented neurons to attend. As will be discussed later in connection with the Goris *et al.* finding [15,28] of facilitation by noise (stochastic resonance), we believe uncertainty reduction is also a viable explanation of that effect as well as for the presence of a dipper function ($\gamma_{\text{eff}}>1$). We are by no means original in suggesting uncertainty as an explanation for findings of the dipper across noise conditions. Pelli [22] fits his data in his Fig. 11 with his uncertainty model and demonstrates the ability of uncertainty to produce the facilitation that is at the left of the dipper. Other mechanisms are needed to produce the threshold elevation that is at the right of the dipper.

There are reports of data that violate the uncertainty hypothesis. For example, Legge *et al.* [21] (p. 400) say "Our data pose an additional problem for the uncertainty model. The model predicts that the slopes of detection psychometric functions should be the same in the presence or absence of external noise. As Table 1 shows, we found lower slopes for detection in noise than for detection in the absence of noise." Their finding a violation of the uncertainty model (also found in their supplemental experiment of their Fig. 7) bothered us for awhile until we realized that their statement is actually a tautology, namely, that there are some experimental conditions and some observers for whom there is minimal uncertainty at the decision stage and these observers will violate the presumption that there is uncertainty.

It is appropriate to bring up the topic of uncertainty in this special issue of JOSAA dedicated to Tanner and Birdsall because of Tanner's contribution to our understanding of uncertainty. The modern history of uncertainty in a signal detection framework began 48 years ago when Tanner pointed out [30] that the finding of an accelerating d' psychometric function does not necessarily imply an intrinsic nonlinear transducer function. The same acceleration could be caused by stimulus uncertainty at the deci-

sion stage. Cohn followed this up in his Ph.D. research at the University of Michigan (with Tanner as an adviser) in the early 1970s with a series of papers in JOSA on signal uncertainty [29,31]. These papers showed a nonlinear d' function that was definitely due to stimulus uncertainty because of controls eliminating alternative mechanisms.

B. Fitting TvN Data

It is easy to get caught up in the minutiae of data and models, so it is useful to step back and take a broad view of what actual TvN data look like and what is needed to fit the data. Since this paper has focused on the versatile PTM model platform, it is useful to look at the type of data that the PTM model was design to fit. Before the Lu and Dosher [5] paper that included double-pass data, the data to be fitted by the PTM were TvN plots of threshold vs. external noise for three d' levels ranging from about 0.5 to 1.5 (2AFC % correct of 65%, 75,% and 85%). A reduced PTM (rPTM in Table 4 of Lu and Dosher [5]) with just four parameters was adequate for fitting the pre-2008 PTM data. The parameters of rPTM were the following: T_{test} (or β) for the $d'=1$ detection threshold and γ for fitting the log–log slope in the 65%–75% range, and a multiplicative noise parameter was needed for adjusting the slope due to the beginning of saturation in the 75%–85% range. A final fourth parameter was needed to adjust the horizontal location of the kink point of the TvN curve. Two additional parameters would have been needed to specify the Birdsall linearization that specifies how the effective γ depends on noise contrast: one to specify the approximate noise contrast at which the linearization takes place and one to specify the extent of the linearization. These last two parameters haven't been needed for fitting Lu and Dosher's data because the shapes of their measured psychometric functions have been relatively independent of the amount of external noise, so the analytic PTM was ideal for their data. It is the stochastic PTM that has problems for fitting that constant shape data.

For the stochastic PTM to fit data when γ is independent of σ_{ext}, rather than introducing a nonlinearity, one could fit the data with a flexible amount of uncertainty. The most detailed study applying the uncertainty model to TvN data was the paper by Eckstein, *et al.* [32]. Lu and Dosher [4] compared the Eckstein, Ahumada, Watson model to the PTM and found them to be similar in fitting the earlier data. Lu and Dosher [5] in their Table 4 compare the PTM to seven other models for fitting their new data and find that the PTM outshines all the other models. The important point to emphasize here is that if the analytic PTM does a good job of fitting the data, then that means shape of the psychometric function is constant-for all noise levels and any four-parameter model that is able to shift the location of the TvN curve (2 parameters) and adjust the spacing of the three d' levels (two more parameters) should do an excellent job of fitting the data. Only if the d' function shape depends on noise strength (a violation of the analytic PTM) or if more types of data are included, such as the double-pass data used by Lu and Dosher [5] would more than four fitting parameters be needed.

C. Birdsall's Theorem

Lu and Dosher [5] (p. 67) point out that Birdsall's theorem rests on the assumption that sources of noise before the dominant nonlinearity are larger than the noise following the nonlinearity. That is correct. However, the nonlinearity might magnify the effectiveness of the input noise, so it might be difficult to compare relative magnitudes of input and output noise. It was for that reason that we carried out simulations for a simple model with a nonlinearity sandwiched between two noise sources. The model that we simulated was the Lu and Dosher [4] PTM because it has been applied to a wide variety of important questions. To our surprise the nonlinearity magnified the effectiveness of the external input noise beyond what we had expected, and in all the simulations presented in Fig. 1 the input noise was able to effectively linearize the system, a feature not present in the analytic version of the PTM. One needs to worry that maybe the multiplicative noise parameter, M_{ext} wasn't strong enough. However, we showed at the end of the Results section (Section 5) that for $M_{\text{ext}}>1.5$ (second row of panels in Fig. 1) the random output noise would have raised thresholds by a greater amount than that indicated by the human efficiency. Yet even with $M_{\text{ext}}=5$, the Birdsall linearization still holds. A similar analysis was done looking at the double-pass results of Lu and Dosher [5] where limits can be placed on the % agreement of the responses when the subjects were shown identical 2AFC stimuli. We showed that the subjects had a sufficiently large percentage of agreements at a $d'=1$ level of performance, that the amount of multiplicative noise could not have been stronger than the levels of our simulations with $M_{\text{ext}}=5$.

The above discussion is about whether the strong Birdsall linearization in our data (see Fig. 2) is compatible with the stochastic PTM of Eq. (4). One should keep in mind that there is a simple alternative to the PTM that allows arbitrary amounts of multiplicative noise and yet is compatible with Birdsall linearization. In the Results Section 5 on amblyopic observers, we introduced the possibility of trial-to-trial fluctuations in the shape of the template [23]. That type of fluctuation results in multiplicative noise that comes *before* the nonlinearity, so Birdsall linearization would be expected. We suspect that the large amounts of multiplicative noise that we find in amblyopes [13,14] together with their strong Birdsall linearization would require some amount of multiplicative noise, such as template instability, to come before the nonlinearity, effectively reducing the value of T_{ext} as seen in Eq. (15).

D. Stochastic Resonance and Uncertainty

The stochastic resonance literature suggests that nonlinear transducer functions will produce facilitation by noise at low d' levels. At Ted Cohn's memorial service one of the authors (SK) focused his talk on the stochastic resonance (SR) research Ted had been doing in the last two years of his life. There is no question that in a system with a hard threshold the presence of noise can act as a pedestal, lifting a very weak signal above threshold. In fact, the left two columns of panels of Fig. 1 (Figs 1(a) and 1(b)) show that the stochastic PTM for low d' levels does show facilitation by noise. This effect has also been found experi-

mentally, first by Blackwell [33] and more recently by Goris *et al.* [28,15]. The same question that came up for the Birdsall effect comes up regarding the mechanism of this facilitation by noise. Is it due to the early nonlinearity such as found in the stochastic PTM or is it due to uncertainty, or both? Cohn believed it was an artifact of uncertainty reduction. He felt that nobody had done sufficiently well-controlled experiments to eliminate the possibility that the accelerated d' function is due to uncertainty reduction rather than to a transducer function with $\gamma>1$. In a posthumously published paper [34] Cohn and colleagues provide the first convincing evidence that SR in a human sensory system is due to uncertainty reduction rather than an accelerated transduction process. The experiments involved detection of a rectangular vibration pulse applied to a finger with and without noise. The somatosensory system was best for this purpose since most of the human SR research has been in the touch system. A 2AFC method was used with both intervals having 300 ms noise bursts and with one of the intervals also having the rectangular pulse. In talks and discussions two years before his article with Perez, Ted had pointed out that an alternative explanation of the SR data could be that the presence of the noise acted to reduce the temporal uncertainty of when the test stimulus would be delivered. He pointed out that a simple control experiment, keeping the noise on continuously, could address this alternative hypothesis. An early nonlinearity explanation would still predict facilitation by the noise, but the uncertainty reduction hypothesis predicts that with continuous noise there would be no SR-like facilitation. That control experiment was performed in the Perez *et al.* [34] paper and the data were clearly in favor of the uncertainty explanation rather than the nonlinear transducer explanation. Blackwell [33] came to a similar conclusion by showing that SR facilitation was present for detection of sinusoids with a noise masker far outside the pass band of the test pattern. This is an excellent argument for facilitation due to reduction of uncertainty in the timing of the stimulus, providing a viable alternative to rectification nonlinearities that enable a PTM type facilitation.

This discussion is relevant to our Birdsall effect investigation for two reasons. First, as pointed out by Lu and Dosher [4,5], the main contender to the PTM model has been the uncertainty model of Eckstein *et al.* [32]. Thus we should remain open minded about the possibility that some amount of uncertainty reduction needs to be included in explanations of the detection of signals in noise when the noise strength is low, as it is in both Birdsall linearization and in facilitation by noise. Second, the theme of the Goris *et al.* [15] paper is given by the title of their paper "Modelling contrast discrimination data suggest both the pedestal effect and stochastic resonance to be caused by the same mechanism." They find that weak amounts of noise produce both some SR facilitation and some Birdsall linearization. They happen to argue in favor of a PTM-like stochastic model or the equivalent gain control model. Goris *et al.* [28] say in their abstract that that "Both simple uncertainty reduction and an energy discrimination strategy can be excluded as possible explanations for this effect" (referring to the SR facilitation by noise). However, in the first section of the Discussion (Section 6) we pointed out a number of aspects of the Goris [15,28] methods that would magnify uncertainty. Until Cohn's simple manipulation of leaving the noise on continuously is carried out, we believe the uncertainty explanation is equally viable. The variability of the Birdsall linearization and the noise facilitation across subjects may favor the uncertainty explanation. We look forward to having this uncertainty of explanations resolved.

E. Multiplicative Noise vs. Saturating Transducer

Behind much of the interest in the shape of the transducer function (c^γ in the present case) and the extent of multiplicative noise is the desire to connect psychophysics to underlying mechanisms that could possibly be tested physiologically. It is thus not surprising that just as this problem has been investigated using the task of detecting signals in noise, it has also been investigated using signals with the same signal as a pedestal. Recently several articles have been published based on the Kontsevich *et al.* [8] (KCT) contrast discrimination dataset. KCT used 2AFC with hundreds of trials at each of more than a dozen pedestal levels. They argued that their data pointed to a large amount of multiplicative noise together with a constantly accelerating transducer function. The ensuing articles pointed out the difficulty of pinning down multiplicative noise vs. a saturating transducer function, especially when based on 2AFC data. Part of the argument hinges on the issue that assuming a particular form for the underlying transducer function (c^γ both for Kontsevich *et al.* and for Lu and Dosher) was much too restrictive. Katkov *et al.* [11] noted that pinning down the amount of multiplicative noise was especially difficult because of an intrinsic nonlinearity in the equations. They argued that the Kontsevich data did not provide evidence for multiplicative noise. Klein [9] agreed that a singularity-like structure was present but that special characteristics of the Kontsevich data provided strong evidence for the presence of multiplicative noise. Klein [10] provided further evidence for multiplicative noise by showing that the Kontsevich data failed a just-noticeable-difference additivity test whereby $d'(AC)=d'(AB)+d'(BC)$ (where A, B, C are contrast levels) if there is no multiplicative noise. We suspect that many of the issues raised in the context of backgrounds known exactly also apply to noise backgrounds.

F. Analytic vs. Stochastic Models

Our analyses in Fig. 1 were based on the fixed-template, trial-by-trial prediction of the underlying stochastic model described in the Dosher and Lu [3] appendix. For all their data fitting however, Lu and Dosher [4,5] make several strong assumptions about the expectation value of non-zero-mean Gaussian noise that is raised to a power. In a footnote to Appendix E, Lu and Dosher [5], p. 80, say

"After nonlinear transduction, the distribution of the external noise might deviate from the Gaussian distribution. However, spatial and temporal summation in the perceptual system should reduce this deviation. When combined with additive and multiplicative noises, both of which are Gaussian distributed, we assume that the sum of the noises is approximately Gaussian. However, we re-

strict ourselves to performance levels below 90% so as to avoid the tails of the distribution."

In our simulations we, too, are combining the signal with large amounts of additive and multiplicative noise. Yet no matter how we manipulate the model, we have found that Birdsall's theorem kicks in at levels much below 90% correct (below $d'=2$). Lu and Dosher commented that spatial and temporal summation in the visual system might convert the first term of Eq. (2) into a Gaussian noise distribution. That would be a miraculous conversion since it could connect the analytic PTM model to the underlying mechanistic model of Eq. (2). However, that connection would involve a transformation of the underlying parameters that is not yet available.

This section will examine the consequences of assuming that $(c_{test}/T_{test}+\sigma_{ext}/T_{ext}\mathbf{R}_1)^{\gamma}$ has an expectation of $(c_{test}/T_{test})^{\gamma}$ and a standard deviation of $k(\sigma_{ext}/T_{ext})^{\gamma}$. That assumption leads to the analytic version of the PTM that Dosher and Lu have applied to numerous situations. Using our notation the analytic d' for the PTM becomes

$$d'^2=(c_{test}/T_{test})^{2\gamma}/[k(\sigma_{ext}/T_{ext})^{2\gamma}+1+M_{test}{}^2(c_{test}/T_{test})^{2\gamma_t}+M_{ext}{}^2(\sigma_{ext}/T_{ext})^{2\gamma}]. \quad (16)$$

The parameter k appears in the denominator because the standard deviation of the Gaussian noise followed by a nonlinearity term introduces a factor that depends on γ. However, for simplicity of notation we follow Lu and Dosher [4] in assuming that $k=1$. The surprise at the end of this section is that no renormalization of parameters is needed in going from the stochastic to the analytic formulae if $d'=1$.

We would now like to invert Eq. (16) from being an expression of d' in terms of c_{test} to an expression of c_{test} in terms of d'. It is not possible to get a simple expression for c_{test} for arbitrary values of γ_t. For that reason we will revert to the original PTM and set $\gamma_t=\gamma$. The analytic PTM prediction for the threshold signal strength at a given d' criterion can then be written as [Lu and Dosher [5] Eq. (14) transformed to our notation]

$$(c_{test}/T_{test})^{2\gamma}=[1+(1+M_{ext}{}^2)(\sigma_{ext}/T_{ext})^{2\gamma}]/(1/d'^2-M_{test}{}^2). \quad (17)$$

The only difference from the Lu–Dosher equation (other than the minor change in variables) is that we have absorbed a factor of $\frac{1}{2}$ into our definition of $M_{test}{}^2$ as discussed earlier. By comparing Eqs. (16) and (17) with the comparable Eqs. (E6) and (E7) of Lu and Dosher [5], we see that their best-fitting parameters for observers CC, SJ, and WC in terms of our parameters are as follows:

	CC	SJ	WC	
$\gamma=\gamma_t$	2.05	2.27	2.36	$=\gamma$,
$T_{test}=$	0.055	0.048	0.086	$=\sigma_{add}{}^{1/\gamma}/\beta$,
$T_{ext}=$	0.103	0.086	0.128	$=\sigma_{add}{}^{1/\gamma}$,
$M_{ext}=$	1.23	0.70	1.60	$=N_{mul}$,
$M_{test}=$	0.33	0.30	0.35	$=N_{mul}(\beta_2/\beta)^{\gamma}/\mathrm{sqrt}(2)$,

(18)

where γ, σ_{add}, N_{mul}, β, and β_2 are the PTM parameters from Table 4 of Lu and Dosher [5]. In the simulations of Fig. 1 the only parameter that can distinguish the stochastic and analytic PTM are γ, M_{ext} and M_{test}. The parameters T_{test} and T_{ext} are always used in conjunction with c_{test} and σ_{ext} and thus simply shift the log–log TvN functions vertically or horizontally without changing shape or relative position in going from the stochastic to the analytic PTM. In the simulations of the middle row of Fig. 1 we have used parameters closely matched to those of the Lu and Dosher data [5] presented in Eq. (18). In the bottom row of Fig. 1 we increased M_{ext} more than threefold to show that Birdsall linearization holds even at those extreme levels.

On pp. 15–16 of Levi *et al.* [14] we showed that Eq. (17) can be rewritten as

$$c_{test}=\mathrm{Th}_0 C(d')F(\sigma_{ext}) \quad (19)$$

where Th_0 is the threshold for $\sigma_{ext}=0$ at $d'=1$ since $C(1)=1$ and $F(0)=1$. Comparing Eqs. (17) and (19) we find

$$\mathrm{Th}_0=T_{test}/(1-M_{test}{}^2)^{1/2\gamma}=0.061,\ 0.053,\ 0.096 \quad \text{for the three observers of Eq. (18).} \quad (20)$$

$$C(d')=((1-M_{test}{}^2)/(1/d'^2-M_{test}{}^2))^{1/2\gamma}. \quad (21)$$

$$F(\sigma_{ext})=(1+(\sigma_{ext}/N_{eq})^{2\gamma}))^{1/2\gamma}, \quad (22)$$

where N_{eq}, similar to the equivalent input noise of a linear amplifier model, is given by

$$N_{eq}=T_{ext}/(1+M_{ext}{}^2)^{1/2\gamma}=0.083,\ 0.079,\ 0.097 \quad \text{for the three observers of Eq. (18).} \quad (23)$$

Levi *et al.* [13,14] showed that N_{eq} is typically very close to the noise detection threshold. The values of N_{eq} for the three observers are quite similar to each other. $C(d')$, the inverse contrast response function, is proportional to the test contrast as a function of d', normalized to unity for $d'=1$. Levi *et al.* [14] not only provide further clarification for this simpler way of expressing the analytic PTM model, but also suggested modifications to Eq. (16) based on their data.

It is worthwhile examining the meaning of the parameters that we have been using, whose best-fitting values for the three Lu and Dosher [5] observers are shown in Eq. (18). T_{test} is very close to the contrast threshold for the Lu and Dosher orientation task. The true threshold at $d'=1$ includes a minor correction term in the denominator of Eq. (20). The horizontal location of the kink point of the TvN curve, obtained by extrapolating its two asymptotes, is given by a simple combination of T_{ext} and M_{ext} as shown in Eq. (23). Finally, the two multiplicative noise terms, M_{test} and M_{ext}, are simply the amount of multiplicative noise when both the test strength and the external noise strength have been normalized to unitless quantities by T_{test} and T_{ext}.

An important outcome of rewriting Eq. (17) in the form of Eq. (19) is that it emphasizes the separability of Eq. (17) into the $C(d')$ term that depends on d' independent of σ_{ext} times the last term of Eq. (19) that depends just on σ_{ext}, independent of d'. This separability means that the

shape of the d' psychometric function should be independent of the external noise. That is clearly not true in our simulations because of Birdsall's theorem, nor is it true in our experimental data. For quite a while we thought the flaw in the logic lay in the assumption made in the text right before Eq. (16) about how to take the expectation values of the nonlinear term. We thought that what was needed were tables of the expectation values and standard deviations of $(k+\mathbf{R})^{\gamma}$, a function of two variables, k and γ. With that knowledge, we believed we could develop an accurate analytic formula to characterize the stochastic PTM. Before continuing with that line of thought, it will be useful to look at predictions of the stochastic and the analytic PTM plotted on top of each other.

Figures 4(a)–4(c) show the analytic PTM on top of the stochastic simulations in a format identical to that of Fig. 1. The only slight changes are as follows:

(a) We use $\gamma_t=2.0$ rather than 1.7 so that $\gamma_t=\gamma$ as in the regular PTM of Lu and Dosher. This choice demonstrates in Fig. 4(a) the sharp saturation of the TvC function, a drawback of the regular PTM.

(b) In Fig. 4(a) we replaced the curve for $\sigma_{\text{ext}}=0.5$ with a curve for $\sigma_{\text{ext}}=0.7$, and we made a comparable shift for the vertical line in Fig. 4(b). The reason for that shift is that the curve for $\sigma_{\text{ext}}=0.5$ in Fig. 4(a) would have overlapped with the curve for $\sigma_{\text{ext}}=0.0$ and not have been visible.

(c) For clarity of presentation the solid thick curves in Figs. 4(a) and 4(b) are for the analytic PTM. The dashed curves are generated by the stochastic PTM of Lu and Dosher [5]. Both calculations are in the Matlab code of Appendix A. We have plotted the curve for $\sigma_{\text{ext}}=0.0$ in Fig. 4(a) with a dashed–dotted line since the analytic formula [Eq. (10)] is identical to the stochastic simulation.

We end this section with a surprise best seen in Fig. 4(b). The curve for $d'=1$ is nearly indistinguishable between the stochastic and analytic models! This striking agreement is so precise only for the case of $\gamma=2$. For other values of γ there is a shift of the TvN curve, and we suspect that the precise agreement between the two curves shifts to a slightly different value of d'. Since threshold is normally defined at $d'=1$ and since values of γ are typically close to 2, this agreement is excellent news for the PTM (at least for $\gamma=2$ and $d'=1$)! The special role of $d'=1$ is also seen in all three panels of Fig. 4(a), where the solid curves (analytic PTM) and the dashed curves (stochastic PTM) all cross each other at $d'=1$.

Also as seen in Fig. 4(b), the difference between the stochastic and the analytic predictions is maximal for zero multiplicative noise ($M_{\text{ext}}=0$, top panels) and vanishes for large values (bottom panels exhibit closer agreement). To see this in Fig. 4(a) it is best to look at the region above $d'=0.5$ since the log–log axes exaggerate differences at

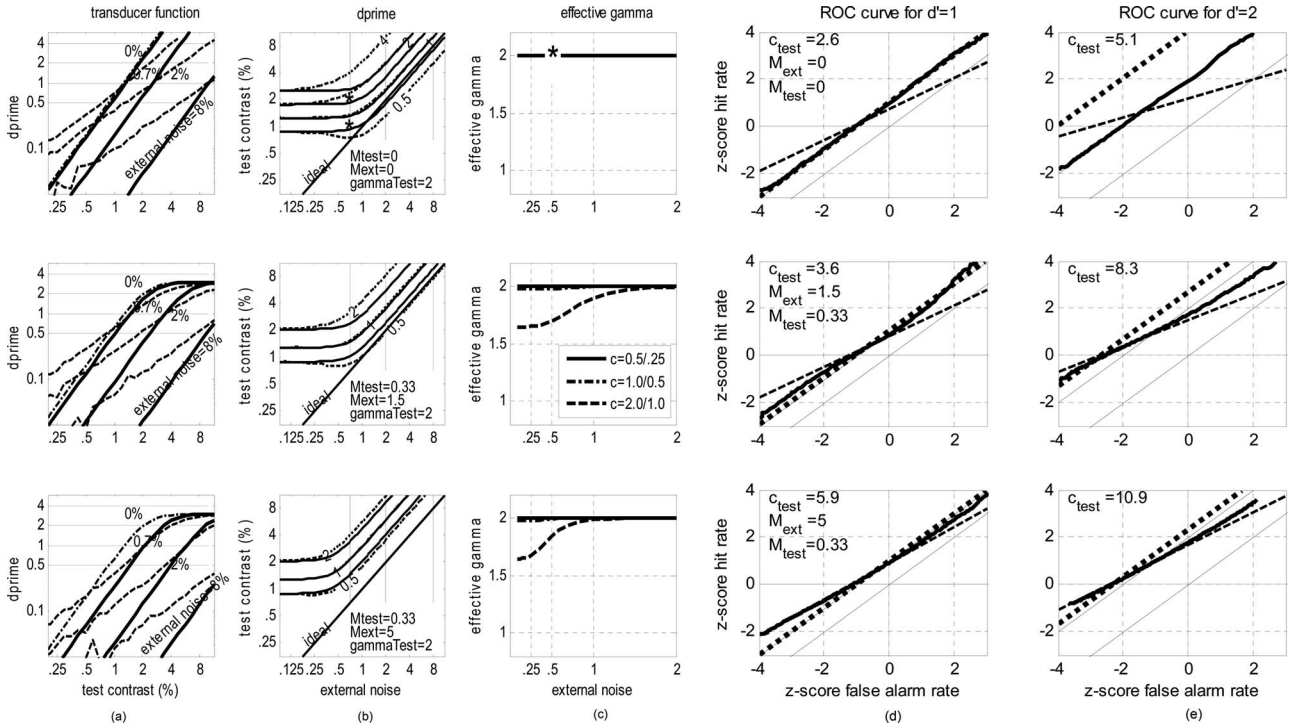

Fig. 4. (a)–(c) are similar to Figs. 1(a)–1(c) except that the analytic PTM of Eqs. (16) and (17) (solid curves) are plotted on top of the stochastic PTM (dotted curves) of Eqs. (4)–(7). Another difference from Fig. 1 is that $\gamma_t=2$ to agree with the original PTM model, giving a hard saturation of the d' function as seen in (a). The remarkable feature of (b) is that the stochastic and analytic models are in excellent agreement for $d'=1$ and $\gamma=2$. Away from the $d'=1$ curve, one sees the effect of Birdsall linearization in that the $d'=0.5$ and 2.0 curves become separated by factors of 2 from the $d'=1$ curve (linearity) for large values of σ_{ext}, whereas at small values of σ_{ext} they are separated by sqrt(2) as expected from a $\gamma=2$ nonlinearity. (c) shows the opposite pattern for the d' exponent for the analytic model from what was seen for the stochastic model of Fig. 1(c). The decrement in exponent at $\sigma_{\text{ext}}=0$ is because of the saturating d' function seen in Fig. 4(a). (d) and (e) show the signal detection ROC plots of the z scores of hit rate vs. false alarm rate for the parameter values indicated in the plot. The thick solid curve is the ROC curve based on the raw data from the simulations of the stochastic PTM. The dotted curve is for the assumptions of the analytic PTM. The dashed curve is based on a Gaussian approximation done by summarizing the simulations in terms of the expected values of the means and standard deviations of the simulations.

low d'. Figure 4(b) also shows that for small values of σ_{ext} the analytic and the stochastic predictions are the same, as expected from Eq. (10). For larger values of σ_{ext}, Birdsall linearization and noise facilitation appear.

The agreement of the analytic and the stochastic PTM at $d'=1$ can be readily understood for zero multiplicative noise ($M_{ext}=M_{test}=0$) as follows: For low values of σ_{ext} both versions must agree with Eq. (10). At large values of σ_{ext} the analytic equation [Eq. (17)] gives $c_{test}/T_{test}=d'^{1/\gamma}\sigma_{ext}/T_{ext}$, while the stochastic PTM after Birdsall linearization gives $c_{test}/T_{test}=d'\sigma_{ext}/T_{ext}$ [Eq. (3)]. Thus they agree for $d'=1$. Only near the kink point will there be a slight, nearly invisible, difference between the two versions. However, for nonzero values of M_{ext} or M_{test} the problem is more challenging since we are no longer able to make a simple transformation to eliminate the nonlinearity. Figures 4(d) and 4(e) present ROC curves that illustrate why the stochastic and analytic formulations are in conflict. An ROC curve is a plot of the z scores of hit vs. false alarm rates. The three rows of panels are for the same conditions as in Figs. 4(a)–4(c) but just for two points of those plots given by $\sigma_{ext}=2$ with $d'=1$ [Fig. 4(d)] and $d'=2$ [Fig. 4(e)]. The value of c_{test} is given by its value in Figs. 4(a) and 4(b) from the stochastic prediction (the prediction with no approximations). The three curves plotted in each panel correspond to three methods for calculating the ROC curves:

Method 1: Stochastic PTM (solid curves). This method is based on histograms of the 50,000 simulation points (see Appendix A) producing probability distribution functions for the blank (false alarms) and the signal (hits) intervals. The ROC curve is a plot of the cumulative hit rate vs. false alarm rate [z scores plotted in Figs. 4(d) and 4(e)].

Method 2: Analytic PTM (dotted curves). The ROC curve is given by $z_{hit}=z_{fa}+d'_{analytic}$ where fa means false alarm, and d' is given by Eq. (16) (with $k=1$ as specified by the analytic PTM).

Method 3: Gaussian approximation to the stochastic PTM (dashed cures). One can improve the analytic PTM by taking expectation values of the mean and standard deviation of the nonlinear term of Eq. (4) and generating an ROC curve given by: $z_{hit}=z_{fa}\sigma_{fa}/\sigma_{hit}+(\mu_{hit}-\mu_{hit})\sigma_{hit}$, where μ_{hit} and σ_{hit} are the mean and the standard deviation of the first term of Eq. (4) and μ_{fa} and σ_{fa} are the same but with $c_{test}=0$. The cross terms of Eq. (4) make $\sigma_{hit}>\sigma_{fa}$ for $\gamma>1$ so the ROC slope of the dashed line is less than 1, even without multiplicative noise. The multiplicative noise terms of Eq. (4) does not alter the ROC curve because we are following the PTM assumption that the multiplicative noise is based on an average stimulus rather than the particular stimulus in the first or second interval.

These ROC curves are generated for a yes–no task of a signal vs. a blank. The 2AFC predictions of d' for relatively straight ROC curve (as ours are) is sqrt(2) times the distance from the origin to the ROC curve [35]. The three plots shown in Fig. 4(d) show that for $d'=1$ the three methods are in quite close agreement. However, the three plots of Fig. 4(e) for $d'=2$, show that the analytic PTM can depart substantially from the correct (stochastic) prediction, as was expected from the previous figures. The Gaussian approximation method also has substantial deviations from the stochastic value. We have not yet been able to find an analytic expression that provides a good approximation to the stochastic model that works both for large external noise where Birdsall linearization occurs and near the kink point where stochastic resonance is found.

By plotting the analytic and the stochastic predictions together as in Fig. 4(b), one obtains a new insight into the stochastic resonance mechanism. In the bottom curves of Fig. 4(b), for $d'=0.5$, facilitation by noise extends beyond the low-noise-contrast regime. Everyone who has found this stochastic resonance facilitation experimentally reports that it is found only at very low noise levels [15,28,29,36]. However, that is because they are comparing thresholds relative to zero-noise performance. If we compare the "true" behavior of the simulation (dotted curves) with the analytic prediction (solid curves) we see that the facilitation begins slightly below the TvN kink point and persists to high external noise. The non-Gaussian nature of the nonlinearity keeps the facilitation persisting in comparison with the outcome for Gaussian noise.

In this paper we did the easy forward model with simulations where we are given a model with known parameters, and we made predictions of d' and % agreement. The greater challenge lies with the inverse problem where one is given the data of d' and % agreement and the goal is to determine the best-fitting model. This is a challenge because there is no way to rapidly calculate the model prediction [unless $\gamma=2$ and $d'=1$ as discussed in connection with Figs. 4(a) and 4(b)]. The standard search for optimal parameters requires many thousands of iterations, so a very rapid model calculation is needed. One can always invent analytic models, but the more ambitious project would be to follow the lead of Lu and Dosher [4] to develop a stochastic model that includes the trial-to-trial dependence on the specific sample of external noise. That model would include improved predictions of classification images and allow for a noisy template before the nonlinearity. A new approach is needed to get a good analytic approximation that includes the nonlinear transforms of random data. The improved analytic approximation would enable efficient data fitting.

7. CONCLUSION AND SUMMARY

We began by citing the revolution in our understanding of detection and identification that took place 50 years ago through the work of Tanner, Birdsall, and colleagues who ushered in our modern understanding of detection of signals in noise. It is interesting that the two compilations of articles of direct relevance to their pioneering work were edited by Ted Cohn. The first was the *Visual Detection* volume [1] that Ted edited, published by the Optical Society of America in 1993. The second, in collaboration with Walter Makous was the compilation of articles 24 years ago in a special issue of JOSAA on Detection and Identification [37]. There were many articles in that special issue of relevance to the present special issue. We will point out a few of them. We already mentioned Smith and

Swift's "Spatial-frequency masking and Birdsall's theorem" on what makes noise noise [16]. Their experiments show how a noise background can be learned so that it acts like a pedestal and can convert linear behavior to power law behavior. The ideal observer article by Geisler and Davila [36] introduced many of us to the distinction between stimuli defined exactly vs. stimuli defined statistically (i.e., with uncertainty). The article on uncertainty by Pelli [22] became the article to read regarding how to deal with uncertainty, including the presence of external noise. Burgess [38] likewise developed his formalism for dealing with uncertainty in handling signals in external noise. Thomas [39] and Klein [40] also dealt with integrating detection and identification into a single framework, similar to the theme of the PTM and the present article. The present special issue of JOSAA, 24 years after the last one on this topic, is likely to remind us once again of the complexity of the visual system and its many still unresolved issues.

As a summary, we point to the various generalizations and clarifications that we have introduced to the Dosher and Lu Perceptual Template Model (PTM): (1) Eq. (5) shows how the test branch for multiplicative noise is able to have an exponent γ_t different from the main exponent. This enables the ability to fit the full TvC psychometric function whether or not noise is present, for both detection and discrimination tasks. (2) Equation (9) shows how the PTM can be converted to a model with gain control replacing multiplicative noise. The equation provides an exact connection, not an approximation. (3) Equation (10) shows how four of the six expanded-PTM parameters can be fixed by the $\sigma_{ext}=0$ portion of the curve. One of the aspects we emphasized in Eq. (2) was to write the PTM in a manner such that each parameter had a direct connection with the data, so that parameter correlations were minimized. (4) By introducing instability of the template, Eq. (15) is able to shift an arbitrary amount of multiplicative noise from following the nonlinearity to preceding it. This enables an increase in the amount of Birdsall linearization. (5) The surprising finding, demonstrated in Fig. 4(b) that the analytic and stochastic PTM predictions are nearly identical for $d'=1$ and $\gamma=2$, was justified based on ROC curves.

There are still many open questions. One critical need is an improved analytic model for fitting joint TvN/TvC data including Birdsall linearization. Our demonstration of their near identity for $d'=1$ and $\gamma=2$ may be a good start for finding a more general formula. The work of Goris *et al.* [28] and Henning and Wichmann [24] point to enhancing the scope of these models to go beyond white noise. They show that notched noise can also lead to linearization of the psychometric function that is likely to be independent of the Birdsall mechanism. Finally, there is the nagging question of why there are so many conflicting results on whether external noise linearizes the psychometric function. We suspect that the resolution to this question will come from future experiments that carefully control the amount of uncertainty, similar to what was done in the paper with Ted Cohn [34] described above.

APPENDIX A

Matlab Program for the Simulations of All 12 Plots of Fig. 1 and 9 Plots of Fig. 4
Note that most of the text items in the plots have been removed to keep the program relatively simple.

```
clear;clf;close all; format compact
gamma=2; gammat=1.7; Ttest=1.25; Text=1;                                  % Fixed parameters
TestContrast=2.^([-2.5:.25:3.5]); c=TestContrast/Ttest;                   % test contrasts
extNoise=2.^([-3.5:.25:3.5]); sigma=extNoise/Text;                        % external noise values
N=50000; Mtest=.33; Mext=1.5;                                             % No. of iterations, multiplicative noise
for in=1:length(extNoise)                                                 % external noise
  for i=1:length(TestContrast)                                            % test contrast
    MultNoise=sqrt (Mext^2*sigma(in)^(2*gamma)+Mtest^2*c(i)^(2*gammat));
    y=sigma(in)*randn(2,N);                                               % The 2 is the 2AFC
    y(1,:)=c(i)+y(1,:);                                                   % add signal to 1st interval
    y2=abs(y).^gamma.*sign(y);                                            % sum of consistent external noise & signal
    y3=y2+randn(2,N)+MultNoise*randn(2,N);                                % add internal & mult random noise
    w1=(y3(1,:)>y3(2,:));                                                 % Number correct
    y3=y2+randn(2,N)+MultNoise*randn(2,N);                                % repeat for double pass
    w2=(y3(1,:)>y3(2,:));                                                 % Number correct on 2nd pass
    p(in,i)=sum(w1+w2)/N/2;                                               % Mean number correct
    agree(in,i)=sum(w2==w1)/N; % Mean                                     % agreement
    danalytic(in,i)=sqrt (c(i)^(2*gamma)/(1+sigma(in)^(2*gamma)+MultNoise^2));  % analytic PTM
  end; end
dprime=erfinv(2*p-1)*2;                                                   % stochastic PTM
Subplot(1, 4, 1)                                                          % Column 1 of figure
loglog(TestContrast,dprime([11 19 27],:),'k,"linewidth,'2.5);hold on      % for the curves with external noise>0
loglog(TestContrast, TestContrast.^gamma./sqrt (1+Mtest^2*
   TestContrast.^(2*gamma)),'k--,' 'linewidth,'2.5)
axis([.2 TestContrast(end)0.2 6])                                         % full frame plot
```

```
subplot(1,4,2); [c,h]=contour (dprime,'[.5 2 2 4],'k,''linewidth,'2.5);hold on;clabel(c,h)      % Column 2
subplot(1,4,2); [c,h]=contour (danalytic,'[.5 1 2 4],'r,''linewidth,'1.5);clabel(c,h)          % Column 2
subplot(1,4,4); [c,h]=contour (agree,'[.52 .62 .72 .8 .9 .99],'k,' 'linewidth,'2.5); clabel(c,h)  % column 4
subplot(1,4,3); effectiveGamma=log (dprime(1:19,[7 11 15])./dprime(1:19,[3 7 11]))/log(2);
ee=extNoise(1:19);                                                                             % Column 3
plot(ee,effectiveGamma(:,1),'k,'ee,effectiveGamma(:,2),'k-,'ee,
    effectiveGamma(:,3),'--k,''linewidth,'2.5);
```

ACKNOWLEDGMENTS

Supported by grants R01EY01728 and R01EY04776 from the National Eye Institute, National Institutes of Health (NIH). We thank the reviewers for their helpful comments. Many discussions with Zhong-Lin Lu have been very helpful in clarifying a number of issues covered in this paper. We also thank Ted Cohn for educating us on many of these interesting topics.

REFERENCES

1. T. E. Cohn, ed., *Visual Detection*, Vol. 3 of Collected Works in Optics (Optical Society of America, 1993).
2. D. J. Lasley and T. E. Cohn, "Why luminance discrimination may be better than detection," Vision Res. **21**, 273–278 (1981).
3. B. A. Dosher and L. L. Lu, "Mechanisms of perceptual attention in precuing of location," Vision Res. **40**, 1269–1292 (2000).
4. Z. L. Lu and B. A. Dosher, "Characterizing human perceptual inefficiencies with equivalent internal noise," J. Opt. Soc. Am. A **16**, 764–778 (1999).
5. Z. L. Lu and B. A. Dosher, "Characterizing observers using external noise and observer models: assessing internal representations with external noise," Psychol. Rev. **115**, 44–82 (2008).
6. J. Nachmias and R. V. Sansbury, "Grating contrast: Discrimination may be better than detection," Vision Res. **14**, 1039–1042 (1974).
7. C. F. Stromeyer and S. A. Klein, "Spatial frequency channels in human vision as asymmetric (edge) mechanisms," Vision Res. **14**, 1409–1420 (1974).
8. L. L. Kontsevich, C. C. Chen, and C. W. Tyler, "Separating the effects of response nonlinearity and internal noise psychophysically," Vision Res. **42**, 1771–1784 (2002).
9. S. A. Klein, "Separating transducer nonlinearities and multiplicative noise in contrast discrimination," Vision Res. **46**, 4279–4293 (2006).
10. S. A. Klein, "A local measure for modeling contrast discrimination, Response to Katkov, Tsodyks and Sagi," Vision Res. **47**, 2912–2917 (2007).
11. M. Katkov, M. Tsodyks, and D. Sagi, "Singularities in the inverse modeling of 2AFC contrast discrimination data," Vision Res. **46**, 259–266 (2006).
12. D. M. Levi and S. A. Klein, "Classification images for detection and position discrimination in the fovea and parafovea," J. Vision **2**, 46–65 (2002).
13. D. M. Levi, S. A. Klein, and I. Chen, "The response of the amblyopic visual system to noise," Vision Res. **47**, 2531–2542 (2007).
14. D. M. Levi, S. A. Klein, and I. Chen, "What limits performance in the amblyopic visual system: seeing signals in noise with an amblyopic brain," J. Vision **8**, 1.1–23 (2008).
15. R. L. Goris, J. Wagemans, and F. A. Wichmann, "Modelling contrast discrimination data suggest both the pedestal effect and stochastic resonance to be caused by the same mechanism," J. Vision **8**, article 17, 1–21 (2008).
16. R. A. Smith and D. J. Swift, "Spatial-frequency masking and Birdsall's theorem," J. Opt. Soc. Am. A **2**, 1593–1599 (1985).
17. G. E. Legge and J. M. Foley, "Contrast masking in human vision," J. Opt. Soc. Am. **70**, 1458–1471 (1980).
18. J. M. Foley, "Human luminance pattern-vision mechanisms: masking experiments require a new model," J. Opt. Soc. Am. A **11**, 1710–1719 (1994).
19. G. E. Legge, D. Kersten, and A. E. Burgess, "Contrast discrimination in noise," J. Opt. Soc. Am. A **4**, 391–404 (1987).
20. J. M. Foley and G. M. Boynton, "Forward pattern masking and adaptation: effects of duration, interstimulus interval, contrast, and spatial and temporal frequency," Vision Res. **33**, 959–980 (1993).
21. A. E. Burgess and B. Colborne, "Visual signal detection. IV. Observer inconsistency," J. Opt. Soc. Am. A **5**, 617–27 (1988).
22. D. G. Pelli, "Uncertainty explains many aspects of visual contrast detection and discrimination," J. Opt. Soc. Am. A **2**, 1508–1532 (1985).
23. W. McIlhagga and A. Paakkonen, "Effects of contrast and length on vernier acuity explained with noisy templates," Vision Res. **43**, 707–716 (2003).
24. G. B. Henning and F. A. Wichmann, "Some observations on the pedestal effect," J. Vision **7**(1): 3, 1–15 (2009).
25. D. Kersten, "Spatial summation in visual noise," Vision Res. **24**, 1977–1990 (1984).
26. T. E. Cohn and D. J. Lasley, "Visual sensitivity," Ann. Rev. Psychol. **37**, 495–521 (1986).
27. R. L. Goris, F. A. Wichmann, and G. B. Henning, "A neurophysiologically plausible population code model for human contrast discrimination," J. Vision **9**(7), 15, 1–22 (2009).
28. R. L. Goris, P. Zaenen, and J. Wagemans, "Some observations on contrast detection in noise," J. Vision **8**(9), 4, 1–15 (2008).
29. T. E. Cohn, L. N. Thibos, and R. N. Kleinstein, "Detectability of a luminance increment," J. Opt. Soc. Am. **64**, 1321–1327 (1974).
30. W. P. Tanner, "Physiological implications of psychophysical data," Ann. N.Y. Acad. Sci. **89**, 752–65 (1961).
31. T. E. Cohn, "Detectability of a luminance increment: Effect of superimposed random luminance fluctuation," J. Opt. Soc. Am. **66**, 1426–1428 (1976).
32. M. P. Eckstein, A. J. Ahumada, and A. B. Watson, "Visual signal detection in structured backgrounds. II. Effects of contrast gain control, background variations, and white noise," J. Opt. Soc. Am. A **14**, 2406–2419 (1997).
33. K. T. Blackwell, "The effect of white and filtered noise on contrast detection thresholds," Vision Res. **38**, 267–280 (1998).
34. C. A. Perez, T. E. Cohn, L. E. Medina, and J. R. Donoso, "Coincidence-enhanced stochastic resonance: experimental evidence challenges the psychophysical theory behind stochastic resonance," Neurosci. Lett. **424**, 31–35 (2007).
35. D. M. Green and J. A. Swets, *Signal Detection Theory and Psychophysics* (Peninsula, 1966).
36. W. S. Geisler and K. D. Davila, "Ideal discriminators in spatial vision: two-point stimuli," J. Opt. Soc. Am. A **2**, 1483–1497 (1985).
37. T. E. Cohn and W. Makous, "Detection and Identification," (Special issue), J. Opt. Soc. Am. A **38**, 1395–1610 (1985).
38. A. E. Burgess, "Double Visual Signal detection: III. On Bayesian use of prior knowledge and cross correlation," J. Opt. Soc. Am. A **2**, 1498–1507 (1985).
39. J. P. Thomas, "Detection and identification: how are they related?" J. Opt. Soc. Am. A **2**, 1457–1467 (1985).
40. S. A. Klein, "Double judgment psychophysics: problems and solutions," J. Opt. Soc. Am. A **2**, 1568–1585 (1985).